

Cooperative Resonances in Light Scattering from Two-Dimensional Atomic Arrays

Ephraim Shahmoon,¹ Dominik S. Wild,¹ Mikhail D. Lukin,¹ and Susanne F. Yelin^{1,2}

¹*Department of Physics, Harvard University, Cambridge Massachusetts 02138, USA*

²*Department of Physics, University of Connecticut, Storrs, Connecticut 06269, USA*

(Received 1 October 2016; revised manuscript received 2 February 2017; published 14 March 2017)

We consider light scattering off a two-dimensional (2D) dipolar array and show how it can be tailored by properly choosing the lattice constant of the order of the incident wavelength. In particular, we demonstrate that such arrays can operate as a nearly perfect mirror for a wide range of incident angles and frequencies, and shape the emission pattern from an individual quantum emitter into a well-defined, collimated beam. These results can be understood in terms of the cooperative resonances of the surface modes supported by the 2D array. Experimental realizations are discussed, using ultracold arrays of trapped atoms and excitons in 2D semiconductor materials, as well as potential applications ranging from atomically thin metasurfaces to single photon nonlinear optics and nanomechanics.

DOI: 10.1103/PhysRevLett.118.113601

Control over propagation and scattering of light fields plays a central role in optical science. In particular, it is well known that emitters exhibit a strongly modified optical response on resonance. For example, enhanced optical scattering in 2D arrays of linearly polarizable elements have been extensively studied in photonics [1–5]. Recently, it has been shown that thin 2D metamaterials, known as metasurfaces, whose constituent elements are optical antennas with varying resonances, can drastically alter the transmitted field by enabling spatial control of its amplitude, phase and polarization [6,7]. As a rule, these elements are microfabricated from macroscopic material, while the separation between the array elements is typically much smaller than the operating wavelength. At the same time, resonant light can be completely reflected by individual atoms when they are strongly coupled to nanophotonic devices with subwavelength localization of light [8–12]. Intuitively, this originates from resonant enhancement of the optical cross section of a polarizable dipole, which at resonance universally scales as λ^2 , λ being its resonant wavelength. Such single atom reflectors yield extraordinary nonlinearities at the level of individual photons [13–15].

Here we explore light scattering from a 2D ordered and dilute array of atoms, with a lattice constant of the order of a wavelength, as can be realized, e.g., using ultracold atoms loaded into optical lattices [16,17]. In such a case near-resonant operation can still lead to strong scattering. Indeed, vanishing transmission at normal incidence was recently discovered in a numerical study of 2D atomic lattices for a specific frequency and lattice arrangement [18]. Because of resonant enhancement, one may naïvely expect that a single layer of dipoles, even if they are as small as individual atoms, may “tile” the plane and thus act as a strong scatterer, provided the density of dipoles exceeds $1/\lambda^2$ [Fig. 1(a)]. This reasoning, though providing intuition for the possibility of strong scattering in dilute

media, ignores the important effect of multiple scattering of electromagnetic fields between the dipoles, associated with dipole-dipole interactions [19–24]. These interactions are crucial to explain the collective phenomena and their tunability explored in this work.

In what follows, we develop an analytical approach to the scattering problem, highlighting the role of the *cooperative resonances* of the dipolar array and their associated collective surface-wave excitations. Strong scattering generically occurs when the frequency of the incident light matches that of the cooperative resonance. The control of scattering off the array can be achieved by adjusting the lattice constant, which determines the cooperative resonances via the underlying dipolar interactions. We demonstrate that the array can

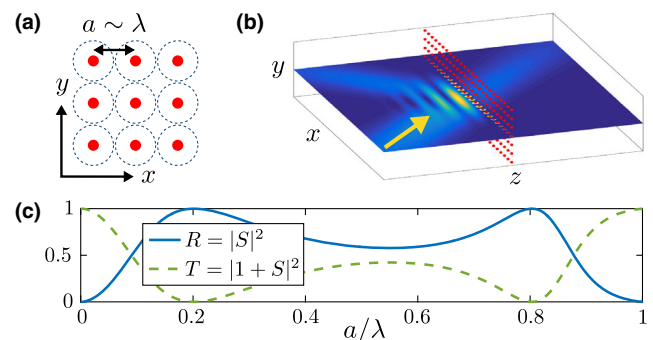


FIG. 1. (a) 2D array of atoms spanning the xy plane at $z = 0$, with interatomic spacing a on the order of the resonant wavelength of the atoms, λ . For resonant light, the individual atomic cross section is of order λ^2 (dashed circles). (b) Light scattering off the array in the single diffraction order regime: The incident field (yellow arrow) produces a forward scattered field at $z > 0$ and a reflected field at $z < 0$. (c) Intensity transmission coefficient T and reflection coefficient R for a square lattice at normal incident and resonant light ($\delta = 0$) as a function of the lattice constant a . Strong scattering is observed with perfect reflection occurring at $a/\lambda \approx 0.2, 0.8$.

form a nearly perfect mirror at almost all incident angles, as well as act as an efficient coupler between an emitter and a collimated optical mode. These results open a new direction in the possibility to mold the flow of light, namely, by using atomically thin metasurfaces.

Scattering at normal incidence.—We consider a 2D array of identical pointlike particles with a generic linear and isotropic polarizability [25]

$$\alpha(\delta) = -\frac{3}{4\pi^2} \epsilon_0 \lambda_a^3 \frac{\gamma/2}{\delta + i(\gamma + \gamma_{nr})/2}. \quad (1)$$

Here, $\delta = \omega - \omega_a$, with $|\delta| \ll \omega_a$, is the detuning between the frequency of the incident light $\omega = 2\pi c/\lambda$ and that of the resonance of the particles $\omega_a = 2\pi c/\lambda_a$, and γ (γ_{nr}) is the radiative (nonradiative) width of this resonance. For a closed cycling transition in atoms we have $\gamma_{nr} = 0$ and the isotropic and linear response corresponds to a $J=0$ to $J=1$ transition far from saturation. The array is taken to be an infinite square lattice with lattice constant $a < \lambda$, spanning the xy plane at $z = 0$ [Fig. 1(a)]. We note that our analysis can be straightforwardly generalized to other lattice geometries.

We first focus on the simplest case of a plane wave at normal incidence. The condition $a < \lambda$ guarantees that only a single diffraction order is present in the far field such that the scattered field on both sides of the array consists of plane waves propagating in the z direction [Fig. 1(b)]. Figure 1(c) shows the transmission and reflection coefficients as a function of the lattice constant, computed for resonant light $\delta = 0$ and in the absence of nonradiative losses, $\gamma_{nr} = 0$, using our analytical approach presented below. We observe that the array scatters strongly over a wide range of lattice constants. In particular, complete reflection (zero transmission) is observed at lattice constants $a/\lambda \approx 0.2, 0.8$. We note that the null transmission at $a/\lambda \approx 0.8$ was also recently found numerically in Ref. [18].

Let us now analyze the above situation. For $a < \lambda$ the total field can be written as

$$\mathbf{E} = [e^{ikz} + S e^{ik|z|}] \mathbf{E}_0, \quad (2)$$

where \mathbf{E}_0 is the amplitude of the field polarized in the xy plane, $k = \omega/c$, and S is a scattering amplitude. For $S = -1$, the transmitted field (at $z > 0$) vanishes and the corresponding perfect reflection gives rise to a standing wave for $z < 0$. The scattering amplitude is determined by the polarization \mathbf{p} induced on the atoms by the incident field, which is identical for all atoms in this case. In turn, \mathbf{p} is the result of multiple scattering of the incident field by all atoms in the array, and it can be characterized by an *effective polarizability* of the atoms defined by $\mathbf{p} = \alpha_e(\delta) \mathbf{E}_0$. A self-consistent solution of this multiple-scattering problem yields [26]

$$S(\delta) = i\pi \left(\frac{\lambda}{a}\right)^2 \frac{\alpha_e(\delta)}{\epsilon_0 \lambda^3} = -\frac{i(\gamma + \Gamma)/2}{\delta - \Delta + i(\gamma + \gamma_{nr} + \Gamma)/2}. \quad (3)$$

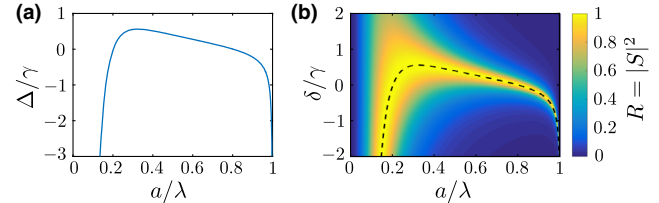


FIG. 2. (a) The cooperative shift Δ , Eq. (4), as a function of the lattice constant a (normal incidence). This plot is central in the design of the scattering since the shift determines the collective resonances of the array according to Eq. (3). Perfect reflection occurs when the cooperative shift equals the incident detuning, $\delta = \Delta$. For example, $\Delta = 0$ at $a/\lambda \approx 0.2, 0.8$ explains the resonances in Fig. 1(c). (b) Intensity reflection coefficient R as a function of lattice constant a and detuning δ . We note that the emerging contour of perfect reflection (bright yellow) coincides with the cooperative resonance plotted in (a) (marked here by the dashed black curve).

By comparing the structure of this linear response to that of an individual atom, Eq. (1), we infer that the dipolar interaction between atoms in the array renormalize both the width γ and the resonant frequency ω_a . They are now supplemented by their cooperative counterparts Γ and Δ , respectively, given by

$$\Delta - \frac{i}{2}\Gamma = -\frac{3}{2}\gamma\lambda \sum_{n \neq 0} G(0, \mathbf{r}_n), \quad \Gamma = \gamma \frac{3}{4\pi} \left(\frac{\lambda}{a}\right)^2 - \gamma. \quad (4)$$

Here, $G(0, \mathbf{r}_n)$ is the transverse component (xx or yy) of the dyadic Green's function of electrodynamics in free space [34], evaluated between the central atom (" $n = 0$ ") at $\mathbf{r}_0 = 0$ and the atom n at \mathbf{r}_n . The explicit expression for Γ holds for $a < \lambda$ and is in fact valid for any 2D lattice [26].

Equation (3) reveals that scattering is strongest when the frequency of the incident light matches the cooperative resonance, $\delta = \Delta$. Perfect reflection ($S = -1$) occurs if, additionally, $\gamma_{nr} = 0$. Therefore, the *key ingredient* that determines the scattering properties of the array is the cooperative dipole-dipole shift Δ , given by the summation (readily evaluated numerically) of the dispersive dipole-dipole shift over all atoms, the real part of Eq. (4). Figure 2(a) provides us with a central tool by which to understand and design the scattering off the array, as it presents the cooperative shift Δ as a function of the lattice constant a [26]. For example, the vanishing cooperative shift Δ at $a/\lambda \approx 0.2, 0.8$ explains the perfect reflection obtained in Fig. 1(c) for $\delta = 0$. Moreover, Fig. 2(b) shows that scattering resonances exist for a wide range of incident field detunings δ near the individual-atom resonance. This is illustrated by Fig. 2(b), in which the reflection coefficient is plotted as a function of both a and δ .

For lossy particles, where $\gamma_{nr} \neq 0$, the scattering amplitude (3) at resonance becomes $S = -(\Gamma + \gamma)/(\Gamma + \gamma + \gamma_{nr})$. Therefore, high reflection requires that radiation damping via scattering is dominant over all other damping sources,

$\gamma + \Gamma \gg \gamma_{\text{nr}}$. The scaling $\gamma + \Gamma \propto (\lambda/a)^2$, originating from cooperative enhancement, then implies that this can be achieved for a sufficiently small lattice constant even if the individual dipoles are poor radiators ($\gamma < \gamma_{\text{nr}}$).

General angle of incidence.—The foregoing analysis can be generalized to all incident angles. We begin by considering $a < \lambda/2$, which ensures a single diffraction order for all incident plane waves, $\mathbf{E}_{0,\mathbf{k}_{\parallel}} e^{i\mathbf{k}_{\parallel} \cdot \mathbf{r}} e^{ik_z z}$, at any angle. Here $\mathbf{k}_{\parallel} = (k_x, k_y, 0)$ denotes the projection of the incident wave vector \mathbf{k} onto the xy plane and $\mathbf{E}_{0,\mathbf{k}_{\parallel}}$ can be decomposed into the two possible transverse polarizations $\mathbf{e}_{p,s}^+ \perp \mathbf{k}$. The total field has the form of Eq. (2), where the scattering amplitude now becomes a 3×3 matrix, and with $e^{i\mathbf{k}_{\parallel} \cdot \mathbf{r}} \mathbf{E}_{0,\mathbf{k}_{\parallel}}$ and k_z replacing \mathbf{E}_0 and k , respectively. The scattering amplitude is again determined by the polarization of the atoms, which is spatially modulated by the in-plane incident wave vector, according to Bloch's theorem. The polarization of atom n can thus be written as $\mathbf{p}_n = \mathbf{p}(\mathbf{k}_{\parallel}) e^{i\mathbf{k}_{\parallel} \cdot \mathbf{r}_n}$, where

$$\mathbf{p}(\mathbf{k}_{\parallel}) = \bar{\alpha}_e(\mathbf{k}_{\parallel}) \mathbf{E}_{0,\mathbf{k}_{\parallel}} \quad (5)$$

denotes the polarization in momentum space. Hence, the effective polarizability is generally defined as the linear response of the polarization of the array in momentum space, given by the tensor

$$\bar{\alpha}_e(\mathbf{k}_{\parallel}) = -\frac{3}{4\pi^2} \epsilon_0 \lambda^3 \frac{\gamma/2}{\delta - \bar{\Delta}(\mathbf{k}_{\parallel}) + i[\gamma + \gamma_{\text{nr}} + \bar{\Gamma}(\mathbf{k}_{\parallel})]/2}. \quad (6)$$

In analogy with Eqs. (1) and (3), $\bar{\Delta}(\mathbf{k}_{\parallel})$ and $\bar{\Gamma}(\mathbf{k}_{\parallel})$ are the cooperative resonance and width tensors, respectively, given in terms of the dyadic Green's function \bar{G} by

$$\bar{\Delta}(\mathbf{k}_{\parallel}) - \frac{i}{2} \bar{\Gamma}(\mathbf{k}_{\parallel}) = -\frac{3}{2} \gamma \lambda \sum_{n \neq 0} \bar{G}(0, \mathbf{r}_n) e^{i\mathbf{k}_{\parallel} \cdot \mathbf{r}_n}. \quad (7)$$

An analytic expression can be obtained for $\bar{\Gamma}$ [26], while $\bar{\Delta}$ has been evaluated numerically.

The scattering amplitude is related to the effective polarizability by an expression similar to that in Eq. (3), from which we can deduce the intensity reflection and transmission coefficients. As illustrated in Fig. 3(a) for s -polarized light, we find that the perfect reflection revealed at cooperative resonance for normal incidence, persists almost completely for all incident angles and both s and p polarizations, well beyond the paraxial regime [26]. This implies that the mirror should operate well for realistic finite size incident beams and arrays, which was further verified for Gaussian beams by a direct numerical approach [26]. The high reflection at oblique angles may again be understood in terms of cooperative resonances of the atom array. For example, in Fig. 3(b) we plot the ss matrix element of $\bar{\Delta}$, which is seen to vary by less than an atomic

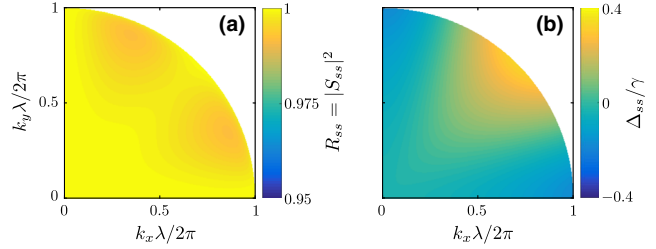


FIG. 3. Scattering at a general angle of incidence for a lattice constant $a = 0.2\lambda$. (a) Intensity reflection coefficient R_{ss} for s -polarized incident and scattered fields at zero detuning from the bare atomic resonance ($\delta = 0$) as a function of the in plane components $k_{x,y}$ of the incident wave vector. (b) ss component of the cooperative shift matrix $\bar{\Delta}$. The variation of the energy shift around the resonance $\Delta_{ss} = \delta = 0$ is small compared to an atomic linewidth, which explains the high reflection R_{ss} at all angles.

linewidth over all incident angles, thus explaining the excellent reflection of s -polarized light.

When the lattice constant exceeds $\lambda/2$, an additional diffraction order can appear. This situation can be analyzed by a straightforward extension of the above formalism, entailing new possibilities such as retroreflection [26].

Surface dipole excitations.—More insight into the physics of the array is gained by noting that the cooperative shift $\bar{\Delta}(\mathbf{k}_{\parallel})$ describes the dispersion relation of collective surface dipole excitations. The nature of these surface modes is revealed by Eq. (5) as the normal modes of the atomic dipoles on the surface, $\mathbf{p}(\mathbf{k}_{\parallel})$. The resonant frequencies of the modes and their corresponding polarizations can be deduced from their linear response $\bar{\alpha}_e(\mathbf{k}_{\parallel})$ in Eq. (6) as the three eigenvalues and eigenvectors of $\bar{\Delta}(\mathbf{k}_{\parallel})$. This interpretation also follows from the quantum master equation governing the dynamics of the atoms, wherein the eigenvalues of $\bar{\Delta}(\mathbf{k}_{\parallel})$ arise naturally as the energies of the Bloch modes of atomic excitations [26]. By diagonalizing $\bar{\Delta}$ for each \mathbf{k}_{\parallel} within the Brillouin zone $k_x, k_y \in [-\pi/a, \pi/a]$, we obtain the band structure of the surface modes shown in Fig. 4(a). The modes around the center of the Brillouin zone (Γ), between the vertical dotted lines, satisfy $|\mathbf{k}_{\parallel}| < 2\pi/\lambda$ and couple to far-field radiation. Therefore, these modes are responsible for the scattering and high reflection discussed above. In contrast, modes with $|\mathbf{k}_{\parallel}| > 2\pi/\lambda$ (beyond the vertical dotted lines) cannot couple to the far field, satisfying $\bar{\Gamma} + \gamma = 0$, and are confined to the surface.

Additional possibilities to control the propagation of light are allowed via *spatial variations* in the 2D atomic array, in analogy to its macroscopic metasurface counterpart. One important example involves the design of a highly directed emission pattern from a single impurity atom coupled to the array. This can be achieved by first analyzing the coupling of the impurity atom to the surface modes, and then introducing a proper spatial modulation to the array,

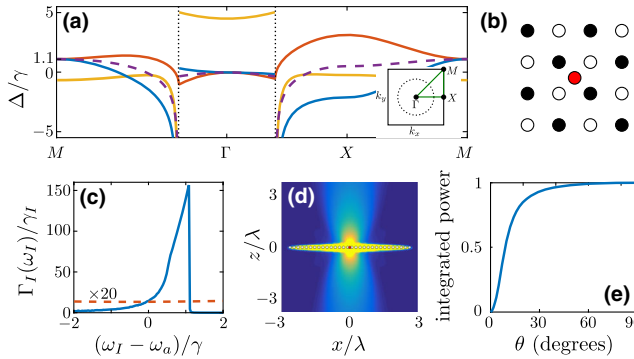


FIG. 4. (a) Band structure of the collective surface modes of the atom array for $a = 0.2\lambda$. The three bands in solid lines correspond to the three eigenvalues of the cooperative shift $\bar{\Delta}(\mathbf{k}_{\parallel})$, whereas the single dashed band is that of array atoms with a single circularly polarized transition, $\mathbf{e}_0 = (1, i, 0)/\sqrt{2}$. The inset shows the location of the special points Γ , X , M in the first Brillouin zone. The dotted vertical lines (main figure) and the circle (inset) indicate the light cone $|\mathbf{k}_{\parallel}| = 2\pi/\lambda$. (b) An impurity atom (red) is placed at the center of the array. The black and white colors of the array atoms represent the two sublattices which form the surface mode M . (c) Decay rate to surface modes inside (dashed) and outside (solid) the light cone, of the impurity atom with polarization $\mathbf{e}_I = (1, -i, 0)/\sqrt{2}$ as a function its transition frequency ω_I . (d) Intensity of the electric field produced by an impurity (red dot), driven at detuning $(\omega - \omega_a)/\gamma = 1.1$ and resonant with the surface modes near the corner of the Brillouin zone (M). An alternating periodic potential, $\delta\omega/\gamma = \pm 0.1$, is applied on an array of 30×30 atoms (white circles), with all other parameters the same as in (b). The bright yellow region near $z = 0$ corresponds to the excited surface modes, which are then coupled into the collimated beam by the periodic potential. (e) Emitted power integrated over a cone of half angle θ for the situation described in (d).

which selectively couples the impurity to a well-collimated, effectively 1D mode.

The decay of an excited impurity atom placed in proximity of the array [Fig. 4(b)] is strongly modified at the cooperative resonance, allowing, e.g., for the excitation of confined surface modes. Assuming, for simplicity, an array of atoms with a single dipolar transition (polarizability) in the direction \mathbf{e}_0 , the dispersion of the surface modes can be described by a single band $\Delta(\mathbf{k}_{\parallel}) = \mathbf{e}_0^\dagger \bar{\Delta}(\mathbf{k}_{\parallel}) \mathbf{e}_0$ [Fig. 4(a), dashed curve]. Within the Born-Markov approximation, the spontaneous emission rate from the impurity atom, with a dipole transition of frequency ω_I , orientation \mathbf{e}_I , and free-space radiative width $\gamma_I < \gamma$, is given by $\Gamma_I(\omega_I) = 3\gamma_I \lambda \text{Im}[\mathbf{e}_I \cdot \mathbf{G}_A(\mathbf{r}_I, \mathbf{r}_I)]$ [34]. Here, $\mathbf{G}_A(\mathbf{r}, \mathbf{r}_I)$ is the electric field produced by a dipole at position \mathbf{r}_I , frequency ω_I and polarization \mathbf{e}_I , which is found, in the presence of the array, using the above formalism [35]. The emission can be decomposed into two contributions: emission into scattering modes ($|\mathbf{k}_{\parallel}| < 2\pi/\lambda$) and into modes confined to the surface ($|\mathbf{k}_{\parallel}| > 2\pi/\lambda$). Its dependence on the impurity's frequency, plotted in Fig. 4(c), exhibits a discontinuity at

$(\omega_I - \omega_a)/\gamma \approx 1.1$, for the given parameters, where emission to the confined modes largely dominates over those scattered to the far field. This discontinuity arises from the resonant excitation of an extremum of the dispersion, corresponding to the surface mode $\mathbf{k}_{\parallel}^M = (\pi/a, \pi, a)$ on the corner of the Brillouin zone (point M) with $\Delta(\mathbf{k}_{\parallel}^M)/\gamma \approx 1.1$. Then, by choosing the impurity transition such that $(\omega_I - \omega_a)/\gamma = 1.1$, the emitted photon is almost entirely confined to propagate along the surface as a polariton with momentum \mathbf{k}_{\parallel}^M .

The mechanism by which this surface polariton can be outcoupled to far-field radiation can be understood as follows. The subradiant mode \mathbf{k}_{\parallel}^M can be thought of as being formed of two degenerate dipolar sublattices of opposite phases, which destructively interfere at the far field [Fig. 4(b)]. Consider now a weak periodic potential which detunes the atoms in the array by $\pm\delta\omega$, where the sign is opposite for any two nearest-neighbor atoms. Such a perturbation splits the degeneracy between the two uniform sublattices, thus allowing them to radiate into a collimated far-field beam. Alternatively, this perturbation can be seen as a spatial modulation of the array structure containing the momentum components $(\pm\pi/a, \pm\pi/a)$, which couple the corner of the Brillouin zone (M) to the center, thus allowing for excitations at \mathbf{k}_{\parallel}^M to be emitted into a well-defined beam normal to the array. Indeed, the numerical simulations for a finite array in Figs. 4(d), 4(e) confirm that the resulting emission is strongly collimated, with $> 90\%$ of the power emitted into a cone of half angle 25° .

Discussion.—The current study demonstrates that the scattering properties of light off a 2D atomic array are determined by the dipolar interactions between the atoms and, in particular, the cooperative resonances.

Possible experimental realizations of the 2D array include ultracold atoms trapped in either red or blue detuned optical lattices [16,36], arrays of plasmonic nanoparticles [2,4], or 2D semiconductors such as monolayers of transition metal dichalcogenides [37], where a lattice structure for the excitons or trions can be created [39–41] (see also Ref. [42]). Considering *disorder* in any of these realizations, we show in Ref. [26] that the cooperative resonances are robust to fluctuations in the atomic positions when the fluctuations are much smaller than the lattice period.

The above results suggest the potential use of such 2D arrays as powerful platforms for classical and quantum optics. In particular, the demonstrated coupling of an emitter to a collimated mode is analogous to efficient coupling to 1D photonic systems. Therefore, it should allow to obtain optical nonlinearities down to a single photon level for properly collimated incident beams [8,13–15,43–46]. Furthermore, the generalization of our approach to other nonhomogeneous arrays may allow to create “atomic-scale metasurfaces” with desired properties. Our work also opens up new prospects in optomechanics. Since the atoms are

very light but at the same time collectively exhibit nearly perfect reflection, they form a highly mechanically susceptible mirror, potentially very useful for the exploration of optomechanics at the quantum level [47].

Finally, we stress the universality of our approach, based on summation of Green's functions at lattice points, relevant for cooperative resonances at any physical system of waves and dipolelike scatterers.

We thank János Perczel for insightful comments concerning the quantum description and dispersion relation of the array. We also acknowledge valuable discussions with Vladimir Shalaev, Markus Greiner, Peter Zoller, Darrick Chang, Hongkun Park, Alex High, and Kristiaan de Greve, and financial support from NSF and the MIT-Harvard Center for Ultracold Atoms.

-
- [1] T. W. Ebbesen, H. J. Lezec, H. F. Ghaemi, T. Thio, and P. A. Wolff, *Nature (London)* **391**, 667 (1998).
 - [2] F. J. García de Abajo, *Rev. Mod. Phys.* **79**, 1267 (2007).
 - [3] S. Xiao and N. A. Mortensen, *Opt. Lett.* **36**, 37 (2011).
 - [4] S. Thongrattanasiri, F. H. L. Koppens, and F. J. García de Abajo, *Phys. Rev. Lett.* **108**, 047401 (2012).
 - [5] S. D. Jenkins and J. Ruostekoski, *Phys. Rev. Lett.* **111**, 147401 (2013).
 - [6] N. Yu and F. Capasso, *Nat. Mater.* **13**, 139 (2014).
 - [7] A. V. Kildishev, A. Boltasseva, and V. M. Shalaev, *Science* **339**, 1232009 (2013).
 - [8] D. E. Chang, A. S. Sørensen, E. A. Demler, and M. D. Lukin, *Nat. Phys.* **3**, 807 (2007).
 - [9] J.-T. Shen and S. Fan, *Phys. Rev. Lett.* **98**, 153003 (2007).
 - [10] A. Asenjo-Garcia, J. D. Hood, D. E. Chang, and H. J. Kimble, *arXiv:1606.04977*.
 - [11] N. V. Corzo, B. Gouraud, A. Chandra, A. Goban, A. S. Sheremet, D. V. Kupriyanov, and J. Laurat, *Phys. Rev. Lett.* **117**, 133603 (2016).
 - [12] H. L. Sørensen, J.-B. Béguin, K. W. Kluge, I. Iakouporov, A. S. Sørensen, J. H. Müller, E. S. Polzik, and J. Appel, *Phys. Rev. Lett.* **117**, 133604 (2016).
 - [13] T. G. Tiecke, J. D. Thompson, N. P. de Leon, L. R. Liu, V. Vuletić, and M. D. Lukin, *Nature (London)* **508**, 241 (2014).
 - [14] I. Shomroni, S. Rosenblum, Y. Lovsky, O. Bechler, G. Guendelman, and B. Dayan, *Science* **345**, 903 (2014).
 - [15] A. Sipahigil, R. E. Evans, D. D. Sukachev, M. J. Burek, J. Borregaard, M. K. Bhaskar, C. T. Nguyen, J. L. Pacheco, H. A. Atikian, C. Meuwly, R. M. Camacho, F. Jelezko, E. Bielejec, H. Park, M. Lončar, and M. D. Lukin, *Science* **354**, 847 (2016).
 - [16] I. Bloch, *Nat. Phys.* **1**, 23 (2005).
 - [17] H. Labuhn, D. Barredo, S. Ravets, S. de Léséleuc, T. Macrì, T. Lahaye, and A. Browaeys, *Nature (London)* **534**, 667 (2016).
 - [18] R. J. Bettles, S. A. Gardiner, and C. S. Adams, *Phys. Rev. Lett.* **116**, 103602 (2016).
 - [19] J. Pellegrino, R. Bourgain, S. Jennewein, Y. R. P. Sortais, A. Browaeys, S. D. Jenkins, and J. Ruostekoski, *Phys. Rev. Lett.* **113**, 133602 (2014).
 - [20] S. D. Jenkins and J. Ruostekoski, *Phys. Rev. A* **86**, 031602(R) (2012).
 - [21] K. Kemp, S. J. Roof, M. D. Havey, I. M. Sokolov, and D. V. Kupriyanov, *arXiv:1410.2497*.
 - [22] M. O. Scully and A. A. Svidzinsky, *Science* **328**, 1239 (2010).
 - [23] R. T. Sutherland and F. Robicheaux, *Phys. Rev. A* **94**, 013847 (2016).
 - [24] K. Kempa, R. Ruppin, and J. B. Pendry, *Phys. Rev. B* **72**, 205103 (2005).
 - [25] P. Lambropoulos and D. Petrosyan, *Fundamentals of Quantum Optics and Quantum Information* (Springer, New York, 2007).
 - [26] See Supplemental Material at <http://link.aps.org/supplemental/10.1103/PhysRevLett.118.113601> for more details, which includes Refs. [27–33].
 - [27] D. P. Craig and T. Thirunamachandran, *Molecular Quantum Electrodynamics* (Academic Press, London, 1984).
 - [28] M. O. Scully and M. S. Zubairy, *Quantum Optics* (Cambridge University Press, Cambridge, England, 1997).
 - [29] R. H. Lehmburg, *Phys. Rev. A* **2**, 883 (1970).
 - [30] M. Kiffner, M. Macovei, J. Eversb, and C. H. Keitel, *Prog. Opt.* **55**, 85 (2010).
 - [31] P. de Vries, D. V. van Coevorden, and A. Lagendijk, *Rev. Mod. Phys.* **70**, 447 (1998).
 - [32] J. A. Klugkist, M. Mostovoy, and J. Knoester, *Phys. Rev. Lett.* **96**, 163903 (2006).
 - [33] M. Antezza and Y. Castin, *Phys. Rev. A* **80**, 013816 (2009).
 - [34] L. Novotny and B. Hecht, *Principles of Nano-Optics* (Cambridge University Press, Cambridge, England, 2006).
 - [35] $\mathbf{G}_A(\mathbf{r}, \mathbf{r}_I)$ is given by the solution for $\mathbf{E}(\mathbf{r})$, with the incident field $\mathbf{E}_0(\mathbf{r})$ being the field produced by the impurity in free-space.
 - [36] T. Kinoshita, T. Wenger, and D. S. Weiss, *Science* **305**, 1125 (2004).
 - [37] Q. H. Wang, K. Kalantar-Zadeh, A. Kis, J. N. Coleman, and M. S. Strano, *Nat. Nanotechnol.* **7**, 699 (2012).
 - [38] H. Li, A. W. Contryman, X. Qian, S. Moeini Ardakani, Y. Gong, X. Wang, J. M. Weisse, C. H. Lee, J. Zhao, P. M. Ajayan, J. Li, H. C. Manoharan, and X. Zheng, *Nat. Commun.* **6**, 7381 (2015).
 - [39] C. Palacios-Berraquero, D. M. Kara, A. R.-P. Montblanch, M. Barbone, P. Latawiec, D. Yoon, A. K. Ott, M. Loncar, A. C. Ferrari, and M. Atatüre, *arXiv:1609.04244*.
 - [40] Y. Lin, X. Ling, L. Yu, S. Huang, A. L. Hsu, Y.-H. Lee, J. Kong, M. S. Dresselhaus, and T. Palacios, *Nano Lett.* **14**, 5569 (2014).
 - [41] S. Zeytinoglu, C. Roth, S. Huber, and A. Imamoğlu, *arXiv:1701.08228*.
 - [42] E. Vetsch, D. Reitz, G. Sagué, R. Schmidt, S. T. Dawkins, and A. Rauschenbeutel, *Phys. Rev. Lett.* **104**, 203603 (2010).
 - [43] A. Goban, C.-L. Hung, S.-P. Yu, J. D. Hood, J. A. Muniz, J. H. Lee, M. J. Martin, A. C. McClung, K. S. Choi, D. E.

- Chang O. Painter, and H. J. Kimble, *Nat. Commun.* **5**, 3808 (2014).
- [45] J. D. Thompson, T. G. Tiecke, N. P. de Leon, J. Feist, A. V. Akimov, M. Gullans, A. S. Zibrov, V. Vuletić, and M. D. Lukin, *Science* **340**, 1202(2013).
- [46] M. Arcari, I. Söllner, A. Javadi, S. Lindskov Hansen, S. Mahmoodian, J. Liu, H. Thyrrstrup, E. H. Lee, J. D. Song, S. Stobbe, and P. Lodahl, *Phys. Rev. Lett.* **113**, 093603 (2014).
- [47] M. Aspelmeyer, T. J. Kippenberg, and F. Marquardt, *Rev. Mod. Phys.* **86**, 1391 (2014).
- [48] A. Srivastava, M. Sidler, A. V. Allain, D. S. Lembke, A. Kis, and A. Imamoğlu, *Nat. Nanotechnol.* **10**, 491 (2015).

Cooperative resonances in light scattering from two-dimensional atomic arrays: Supplemental Material

Ephraim Shahmoon,¹ Dominik S. Wild,¹ Mikhail D. Lukin,¹ and Susanne F. Yelin^{1,2}

¹*Department of Physics, Harvard University, Cambridge MA 02138, USA*

²*Department of Physics, University of Connecticut, Storrs, Connecticut 06269, USA*

(Dated: February 17, 2017)

This Supplementary document is organized as follows. Sec. 1 reviews the general approach we use for the scattering problem by an array of dipole scatterers. Sec. 2 is dedicated for the derivation of our analytical formulation of scattering by a 2D lattice, including its quantum version. Sec. 3 and 4 discuss in more depth some of the results and consequences that emerge from our analytical treatment. Finally, Sec. 5 presents the direct numerical approach we employ to verify our theoretical results in a realistic finite size scenario.

1. THE SCATTERING PROBLEM: GENERAL APPROACH

We consider the scattering of a general incident electric field by a collection of atoms modeled as point-like dipole scatterers characterized by their linear polarizability. This description naturally applies for the scattering due to the electric linear response of any collection of scatterers which are much smaller than the incident wavelength, such as atoms in the optical frequency domain, and has been used before by many authors in the photonics community, e.g. for the treatment of light scattering by arrays of nano-particles [1].

1.1. Electromagnetic scattering theory

Assuming an incident field $\mathbf{E}_0(\mathbf{r})$ and atoms $n = 1, \dots, N$ at positions \mathbf{r}_n , the goal is to find the electric field at any given point \mathbf{r} . As usual, we begin with Maxwell's curl equations for fields at frequency $\omega = kc = k/\sqrt{\epsilon_0\mu_0}$, obtaining the wave equation

$$\nabla \times \nabla \times \mathbf{E} - k^2 \mathbf{E} = \frac{k^2}{\epsilon_0} \mathbf{P}, \quad (\text{S1})$$

whose formal solution is

$$E_i(\mathbf{r}) = E_{0,i}(\mathbf{r}) + \frac{k^2}{\epsilon_0} \sum_j \int_V d\mathbf{r}' G_{ij}(k, \mathbf{r}, \mathbf{r}') P_j(\mathbf{r}'), \quad (\text{S2})$$

with $A_i = \mathbf{e}_i \cdot \mathbf{A}$ the $i = x, y, z$ component of a vector \mathbf{A} and where $G_{ij}(k, \mathbf{r}, \mathbf{r}')$ is the Green's function of Eq. (S1), namely, the i component of the electric field (in inverse length units) produced by a delta-function source at \mathbf{r}' polarized on the j axis; in free space this so-called dyadic Green's function takes the form [2]

$$G_{ij}(k, \mathbf{r}_1, \mathbf{r}_2) = \frac{e^{ikr}}{4\pi r} \left[\left(1 + \frac{ikr - 1}{k^2 r^2} \right) \delta_{ij} + \left(-1 + \frac{3 - 3ikr}{k^2 r^2} \right) \frac{r^i r^j}{r^2} \right], \quad (\text{S3})$$

with $\mathbf{r} = \mathbf{r}_1 - \mathbf{r}_2$, $r = |\mathbf{r}|$ and $r^i = \mathbf{e}_i \cdot \mathbf{r}$.

Considering now that polarization \mathbf{P} exists only on the atoms and using their linear response $\alpha(\omega)$ (generally a tensor, but taken as scalar/isotropic and identical for all atoms), we have

$$\mathbf{P}(\mathbf{r}) = \sum_{n=1}^N \alpha \mathbf{E}(\mathbf{r}) \delta(\mathbf{r} - \mathbf{r}_n), \quad (\text{S4})$$

so that Eq. (S2) becomes

$$E_i(\mathbf{r}) = E_{0,i}(\mathbf{r}) + 4\pi^2 \frac{\alpha}{\epsilon_0 \lambda^3} \sum_j \sum_n \lambda G_{ij}(k, \mathbf{r}, \mathbf{r}_n) E_j(\mathbf{r}_n), \quad (\text{S5})$$

where $\lambda = 2\pi/k$. Eq. (S5) has a Lippman-Schwinger form, and together with the Green's function, Eq. (S3), it forms the formal solution and the starting point of our scattering theory. The idea is to self-consistently evaluate the

fields $E_j(\mathbf{r}_n)$, or more precisely the polarizations $p_j(\mathbf{r}_n) = \alpha E_j(\mathbf{r}_n)$, at the atomic positions $\mathbf{r} = \mathbf{r}_n$, which in turn determine the right-hand side of the equation, thus allowing for the solution of the field at any point, $E_i(\mathbf{r})$ at the left-hand side of the equation. Writing Eq. (S5) at an atomic position $\mathbf{r} = \mathbf{r}_n$, we obtain a self-consistent equation for the polarization induced on the atoms $p_i^n = \alpha E_i(\mathbf{r}_n)$,

$$p_i^n = p_{0,i}^n + \sum_{m \neq n} \sum_j 4\pi^2 \frac{\alpha}{\varepsilon_0 \lambda^3} \lambda G_{ij}^{nm} p_j^m, \quad (\text{S6})$$

with $p_{0,i}^n = \alpha E_{0,i}(\mathbf{r}_n)$ and $G_{ij}^{nm} = G_{ij}(k, \mathbf{r}_n, \mathbf{r}_m)$. Here the summation over atoms (index m) skips the atom n at which we evaluate the field, in accordance with the convention we adopt for the atomic polarizability, as explained below. The idea is that by inserting the solution of Eq. (S6) into Eq. (S5), we obtain the field at any point $E_i(\mathbf{r})$.

The solution of Eq. (S6) and then of Eq. (S5) can be readily performed numerically for any general case of incident field and finite collection of atoms, as we show in Sec. 5 below. Nevertheless, by exploiting the symmetry of an ordered array, an analytical solution can be obtained, as shown in Sec. 2 (similar to the approach taken in Ref. [1]).

1.2. The atomic polarizability

Considering a $J = 0$ to $J = 1$ transition of an atom with a dipole matrix element d and frequency ω_a the linear polarizability is given by [3, 4]

$$\alpha(\omega) = \frac{2d^2\omega_a}{\hbar} \frac{1}{\omega_a^2 - \omega^2 - i\gamma_0\omega}, \quad (\text{S7})$$

where γ_0 is a damping term which is addressed below. It is worth recalling here that a similar form of polarizability is found for classical systems alike, so that our discussion is kept general for all point-like polarizable scatterers in their linear regime. For small detuning $\delta = \omega - \omega_a$ with respect to ω_a , $|\delta| \ll \omega_a$, and using the spontaneous emission rate of a single atom $\gamma = d^2\omega_a^3/(3\pi\varepsilon_0\hbar c^3)$, we obtain

$$\alpha(\omega) = -\frac{3}{4\pi^2} \varepsilon_0 \lambda_a^3 \frac{\gamma/2}{\delta + i\gamma_0/2}. \quad (\text{S8})$$

Skipping the $m = n$ term in the sum of Eq. (S6) implies that the radiative damping γ of an individual atom is included in the total damping γ_0 . Namely,

$$\gamma_0 = \gamma + \gamma_{\text{nr}}, \quad (\text{S9})$$

where γ_{nr} denotes the non-radiative loss rate. This also implies that ω_a already includes the Lamb shift correction (or that we neglect it). We note, that one may choose to include the $m = n$ term in Eq. (S6) by neglecting the real part of G_{ij}^{nn} (neglecting the Lamb shift) and taking $\gamma_0 = \gamma_{\text{nr}}$, yielding exactly the same results for p_i^n and $E_i(\mathbf{r})$.

2. ANALYTICAL APPROACH

2.1. Polarization built on the atoms

We consider an infinite array of atoms spanning the xy plane at $z = 0$ and illuminated by an incident field represented by its decomposition to plane waves $\mathbf{E}_0(\mathbf{r}) = \sum_{\mathbf{k}_{\parallel}} \mathbf{E}_{0,\mathbf{k}_{\parallel}} e^{i\mathbf{k}\cdot\mathbf{r}}$. The wavevector of each plane wave is characterized by its projections on the xy plane and z axis, \mathbf{k}_{\parallel} and $k_z = \sqrt{k^2 - |\mathbf{k}_{\parallel}|^2}$, respectively, whereas its amplitude $\mathbf{E}_{0,\mathbf{k}_{\parallel}}$ is spanned by the two transverse polarizations $\mathbf{e}_{p,s}^+ \perp \mathbf{k}$. At normal incidence ($\mathbf{k}_{\parallel} = 0$) we have $k_z = k$ and the field is polarized in the xy plane, $\mathbf{e}_{p,s}^+ \in \{\mathbf{e}_x, \mathbf{e}_y\}$.

In order to exploit the discrete translational symmetry of the lattice (as in the Bloch theorem), we define the 2D Fourier transform of a function $f(\mathbf{r})$ sampled at the lattice sites n , $f_n = f(\mathbf{r}_n)$, as

$$f(\mathbf{k}_{\parallel}) = \frac{1}{N} \sum_{n=1}^N e^{-i\mathbf{k}_{\parallel} \cdot \mathbf{r}_n} f_n, \quad f_n = N A_0 \int_{\text{BZ}} \frac{d\mathbf{k}_{\parallel}}{(2\pi)^2} e^{i\mathbf{k}_{\parallel} \cdot \mathbf{r}_n} f(\mathbf{k}_{\parallel}), \quad (\text{S10})$$

where A_0 is the area of the lattice unit cell and BZ means that the integral over \mathbf{k}_{\parallel} is performed within the first Brillouin zone of the reciprocal lattice. For a square lattice, $\mathbf{r}_n = \mathbf{r}_{n_x, n_y} = a(n_x \mathbf{e}_x + n_y \mathbf{e}_y)$, we have $A_0 = a^2$ and $\int_{\text{BZ}} d\mathbf{k}_{\parallel} = \int_{-\pi/a}^{\pi/a} dk_x \int_{-\pi/a}^{\pi/a} dk_y$. Applying this Fourier transformation on Eq. (S6) we find

$$\mathbf{p}(\mathbf{k}_{\parallel}) = \alpha \mathbf{E}_{0, \mathbf{k}_{\parallel}} + 4\pi^2 \frac{\alpha}{\varepsilon_0 \lambda^3} \lambda \bar{g}(\mathbf{k}_{\parallel}) \mathbf{p}(\mathbf{k}_{\parallel}) \quad (\text{S11})$$

for each \mathbf{k}_{\parallel} value contained in the incident field, where

$$\bar{g}(\mathbf{k}_{\parallel}) = \sum_{n \neq 0} \bar{G}(0, \mathbf{r}_n) e^{-i\mathbf{k}_{\parallel} \cdot \mathbf{r}_n}, \quad (\text{S12})$$

also noting the fact that the dyadic Green's function in free space, $\bar{G}(\mathbf{r}, \mathbf{r}')$ depends only on the difference $\mathbf{r} - \mathbf{r}'$, see Eq. (S3). The solution of (S11) is then

$$\begin{aligned} \mathbf{p}_n &= \sum_{\mathbf{k}_{\parallel}} \mathbf{p}(\mathbf{k}_{\parallel}) e^{i\mathbf{k}_{\parallel} \cdot \mathbf{r}_n}, \\ \mathbf{p}(\mathbf{k}_{\parallel}) &= \bar{\alpha}_e(\mathbf{k}_{\parallel}) \mathbf{E}_{0, \mathbf{k}_{\parallel}}, \end{aligned} \quad (\text{S13})$$

with the effective polarizability tensor

$$\bar{\alpha}_e(\mathbf{k}_{\parallel}) = -\frac{3}{4\pi^2} \varepsilon_0 \lambda_a^3 \frac{\gamma/2}{\delta - (\lambda_a/\lambda)^3 \bar{\Delta}(\mathbf{k}_{\parallel}) + i[\gamma + \gamma_{\text{nr}} + (\lambda_a/\lambda)^3 \bar{\Gamma}(\mathbf{k}_{\parallel})]/2}, \quad (\text{S14})$$

and the collective radiative response from Eq. (7) of the main text, namely,

$$\bar{\Delta}(\mathbf{k}_{\parallel}) = -\frac{3}{2} \gamma \lambda \text{Re}[\bar{g}(\mathbf{k}_{\parallel})], \quad \bar{\Gamma}(\mathbf{k}_{\parallel}) = 3\gamma \lambda \text{Im}[\bar{g}(\mathbf{k}_{\parallel})]. \quad (\text{S15})$$

Finally, the effective polarizability from Eq. (6) of the main text is reached by taking $\lambda_a^3/\lambda^3 \approx 1$ in Eq. (S14). We note that Eq. (S13) implies that the polarization built on the atomic array due to an incident plane wave with in-plane wavevector \mathbf{k}_{\parallel} is not mixed with that induced by a different wavevector, and that the *collective* response of the array polarization to a field with a given wavenumber \mathbf{k}_{\parallel} is described by the effective polarizability $\bar{\alpha}_e(\mathbf{k}_{\parallel})$.

The result at normal incidence, Eq. (3) in the main text, is obtained by noting that the sum $\bar{g}(0)$ for $\mathbf{k}_{\parallel} = 0$ in Eq. (S12) is symmetric in the x and y directions due to the structure of \bar{G} from Eq. (S3) and the symmetry of the lattice. Therefore, the tensor \bar{g} becomes diagonal $g_{ij} = \delta_{ij} g_i$ with $g_x = g_y$. At normal incidence the field is polarized in the xy plane so that \bar{g} effectively appears as a scalar, $g_x = \sum_{n \neq 0} G_{xx}(0, \mathbf{r}_n)$, and the collective response becomes $\Delta - i\Gamma/2 = -(3/2)\gamma \lambda g_x$.

2.2. Calculation of the cooperative shift and width

Both $\bar{\Delta}$ and $\bar{\Gamma}$ can be obtained by a direct numerical summation over the atomic lattice points, as in Eq. (S15). Alternatively, one can begin by representing the sum $\bar{g}(\mathbf{k}_{\parallel})$ in 2D reciprocal (wavevector) space by using the relation [2]

$$G_0(x, y, z) = \frac{e^{ik\sqrt{x^2+y^2+z^2}}}{4\pi\sqrt{x^2+y^2+z^2}} = \frac{i}{8\pi^2} \int d\mathbf{k}'_{\parallel} e^{-i\mathbf{k}'_{\parallel} \cdot \mathbf{r}_{\parallel}} \frac{e^{ik'_z|z|}}{k'_z}, \quad (\text{S16})$$

where $\mathbf{r}_{\parallel} = (x, y)$ and $k'_z = \sqrt{k^2 - |\mathbf{k}'_{\parallel}|^2}$. Then, writing

$$g_{ij}(\mathbf{k}_{\parallel}) = \sum_n \int d\mathbf{r}_{\parallel} G_{ij}(0, \mathbf{r}_{\parallel}) e^{-i\mathbf{k}_{\parallel} \cdot \mathbf{r}_{\parallel}} \delta(\mathbf{r}_{\parallel} - \mathbf{r}_n) - G_{ij}(0, 0) \quad (\text{S17})$$

(recalling that \mathbf{r}_n only exists on the xy plane), and using $G_{ij} = [\delta_{ij} + (1/k^2)\partial_i \partial_j]G_0$, we find

$$g_{ij}(\mathbf{k}_{\parallel}) = \begin{cases} \frac{i}{8\pi^2} \int d\mathbf{k}'_{\parallel} \frac{1}{k'_z} \left(\delta_{ij} - \frac{k'_i k'_j}{k^2} \right) \sum_n \int d\mathbf{r}_{\parallel} \delta(\mathbf{r}_{\parallel} - \mathbf{r}_n) e^{-i(\mathbf{k}'_{\parallel} + \mathbf{k}_{\parallel}) \cdot \mathbf{r}_{\parallel}} - \frac{i}{3\lambda} \delta_{ij}, & \text{for } i, j = \{x, y\} \cup i = j = z, \\ -\frac{i}{3\lambda} \delta_{ij}, & \text{otherwise.} \end{cases} \quad (\text{S18})$$

Here we used $G_{ij}(0,0) = \frac{i}{3\lambda} \delta_{ij}$ obtained by taking the $\mathbf{r} \rightarrow 0$ limit of $G_{ij}(\mathbf{r},0)$ and neglecting its real part (associated with the Lamb shift of the atomic resonance ω_a). We may now introduce the reciprocal lattice as the Fourier transform of the atomic lattice structure

$$\rho(\mathbf{k}'_{\parallel}) = \int d\mathbf{r}_{\parallel} e^{-i\mathbf{k}'_{\parallel} \cdot \mathbf{r}_{\parallel}} \sum_n \delta(\mathbf{r}_{\parallel} - \mathbf{r}_n) = \frac{(2\pi)^2}{A_0} \sum_m \delta(\mathbf{k}'_{\parallel} - \mathbf{q}_m), \quad (\text{S19})$$

which forms a lattice in 2D wavevector space at lattice points \mathbf{q}_m (wavevectors) satisfying $\mathbf{q}_m \cdot \mathbf{r}_n = 2\pi M$ with an integer M and for any n and m . Using Eq. (S19) in (S18) we obtain

$$g_{ij}(\mathbf{k}_{\parallel}) = \frac{i}{2A_0} \sum_m \frac{1}{\sqrt{k^2 - |\mathbf{q}_m - \mathbf{k}_{\parallel}|^2}} \left[\delta_{ij} - \frac{(\mathbf{q}_m - \mathbf{k}_{\parallel})_i (\mathbf{q}_m - \mathbf{k}_{\parallel})_j}{k^2} \right] - \delta_{ij} \frac{i}{3\lambda}, \quad (\text{S20})$$

valid for $i,j = \{x,y\}$ or $i = j = z$ whereas $g_{ij}(\mathbf{k}_{\parallel}) = -\delta_{ij} \frac{i}{3\lambda}$ otherwise. For the square lattice we have $\mathbf{q}_{m_x,m_y} = (2\pi/a)(m_x \mathbf{e}_x + m_y \mathbf{e}_y)$ and the unit cell area is $A_0 = a^2$ so that Eq. (S20) becomes

$$g_{ij}(\mathbf{k}_{\parallel}) = \frac{i}{2a^2} \sum_{m_x=-\infty}^{\infty} \sum_{m_y=-\infty}^{\infty} \frac{(\delta_{ij} - [(2\pi/a)m_x - k_x][(2\pi/a)m_y - k_y]/k^2)}{\sqrt{k^2 - [(2\pi/a)m_x - k_x]^2 - [(2\pi/a)m_y - k_y]^2}} - \delta_{ij} \frac{i}{3\lambda}. \quad (\text{S21})$$

The sums in Eqs. (S20,S21) can be used for a numerical evaluation of \bar{g} (and hence of $\bar{\Delta}$ and $\bar{\Gamma}$) in momentum space, instead of to the sum (S12) that is performed in real space. This is achieved by using a proper regularization and renormalization procedure [5]. More importantly, this form of \bar{g} can be used to find an analytical expression for $\bar{\Gamma}$ in the single diffraction order case. Considering only the imaginary part of g_{ij} in Eq. (S21), the square root in the denominator has to be real. Since this square root originates in the wavenumber in the z direction, k_z' that appears in the wave expansion of the Green's function (Eqs. S16 and S18), this requirement means that radiation damping (imaginary part of g_{ij}) is related to waves that can propagate out of the atomic array. Taking for example $k_y = 0$, we have $|k_x - m_x 2\pi/a| < k$ and $|k_x| < k$, leading to $|m_x| < 2a/\lambda$ (for $k_y \neq 0$ this condition on m_x becomes even more restrictive). Then, for the case $a < \lambda/2$ and for any (k_x, k_y) , only the zeroth-order diffraction $m_x = m_y = 0$ contributes to radiation and damping. At normal incidence $k_x = k_y = 0$, such single diffraction order exists for $a < \lambda$ as can be inferred from the condition on m_x . Similar conclusions are reached for any lattice structure considering Eq. (S20). Then, from Eq. (S15) we obtain

$$\Gamma_{ij} = \gamma \frac{3}{4\pi} \left(\frac{\lambda}{a} \right)^2 \frac{k}{k_z} \left(\delta_{ij} - \frac{k_i k_j}{k^2} \right) - \gamma \delta_{ij}, \quad (\text{S22})$$

again valid for $i,j \in \{x,y\}$ or $i = j = z$, while $\Gamma_{ij} = -\gamma \delta_{ij}$ otherwise. At normal incidence we have $k_x = k_y = 0$ and $k_z = k$ leading to $\Gamma = \Gamma_{xx} = \gamma \frac{3}{4\pi} \frac{\lambda^2}{a^2} - \gamma$ as in Eq. (4) of the main text. For larger values of a more diffraction orders appear, and analytical results for their contribution to $\bar{\Gamma}$ are obtained in the same way.

2.3. The scattered field

Let us now find the scattered field due to a given plane wave component of the incident field $\mathbf{E}_{0,\mathbf{k}_{\parallel}} e^{i\mathbf{k} \cdot \mathbf{r}}$ with an in-plane wavevector \mathbf{k}_{\parallel} . Returning to Eq. (S5), we use $\mathbf{E}^n = \mathbf{p}^n / \alpha = \bar{\alpha}_e(\mathbf{k}_{\parallel}) \mathbf{E}_{0,\mathbf{k}_{\parallel}} e^{i\mathbf{k}_{\parallel} \cdot \mathbf{r}_n} / \alpha$ in the right-hand side, and obtain

$$\mathbf{E}(\mathbf{r}) = \mathbf{E}_{0,\mathbf{k}_{\parallel}} e^{i\mathbf{k}_{\parallel} \cdot \mathbf{r}} e^{ik_z z} + 4\pi^2 \lambda \bar{g}_{sc}(\mathbf{k}_{\parallel}, \mathbf{r}) \frac{\bar{\alpha}_e(\mathbf{k}_{\parallel})}{\varepsilon_0 \lambda^3} \mathbf{E}_{0,\mathbf{k}_{\parallel}}, \quad (\text{S23})$$

with

$$\bar{g}_{sc}(\mathbf{k}_{\parallel}, \mathbf{r}) = \sum_n \lambda \bar{G}(\mathbf{r}, \mathbf{r}_n) e^{i\mathbf{k}_{\parallel} \cdot \mathbf{r}_n}. \quad (\text{S24})$$

Using again the above methods [the expansion (S16) and the reciprocal lattice (S19)] we find

$$g_{sc,ij}(\mathbf{k}_{\parallel}, \mathbf{r}) = \frac{i}{2A_0} \sum_m \frac{1}{\sqrt{k^2 - |\mathbf{k}_{\parallel} + \mathbf{q}_m|^2}} \left[\delta_{ij} - \xi_{ij} \frac{(\mathbf{k}_{\parallel} + \mathbf{q}_m)_i (\mathbf{k}_{\parallel} + \mathbf{q}_m)_j}{k^2} \right] e^{i(\mathbf{k}_{\parallel} + \mathbf{q}_m) \cdot \mathbf{r}_{\parallel}} e^{i\sqrt{k^2 - |\mathbf{k}_{\parallel} + \mathbf{q}_m|^2} |z|}, \quad (\text{S25})$$

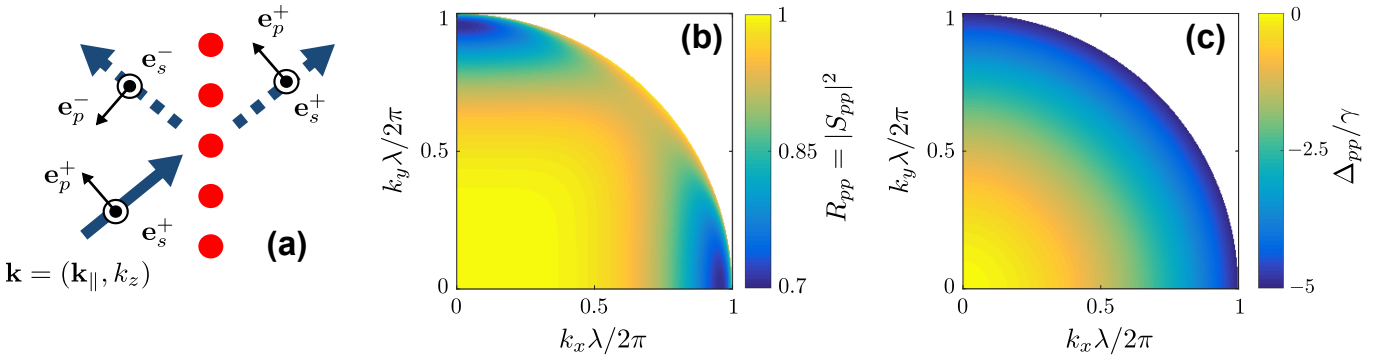


FIG. S1: (a) Scattering at a general angle of incidence. The polarizations of incident and forward scattered fields with wavevector \mathbf{k} are spanned by the forward basis $\mathbf{e}_{p,s}^+ \perp \mathbf{k}$, whereas that of the reflected field is spanned by the backward polarization basis $\mathbf{e}_{p,s}^- \perp \mathbf{k}$. (b) Intensity reflection coefficient R_{pp} for p -polarized incident and scattered fields at zero detuning from the bare atomic resonance ($\delta = 0$) as a function of the in plane components $k_{x,y}$ of the incident wavevector. The lattice constant is $a = 0.2\lambda$. (c) pp component of the cooperative shift matrix $\bar{\Delta}$ (see Sec. 3.2 below).

with \mathbf{r}_{\parallel} and z the projections of \mathbf{r} along the xy plane and the z axis, respectively, and where $\xi_{ij} = -1$ for either $i = z \cap j \neq z$ or $j = z \cap i \neq z$ at $z < 0$, and $\xi_{ij} = 1$ otherwise. For a square lattice we have as usual $A_0 = a^2$, $\sum_m \rightarrow \sum_{mx=-\infty}^{\infty} \sum_{my=-\infty}^{\infty}$ and $\mathbf{q}_m \rightarrow (2\pi/a)(m_x \mathbf{e}_x + m_y \mathbf{e}_y)$. Therefore, the field scattered from all atoms to a point \mathbf{r} , represented by the sum $\bar{g}_{sc}(\mathbf{k}_{\parallel}, \mathbf{r})$ from Eq. (S24), is revealed by Eq. (S25) to be a sum of plane wave contributions from all diffraction orders m with wavevectors $\mathbf{k}_{\parallel} + \mathbf{q}_m$ and $\sqrt{k^2 - |\mathbf{k}_{\parallel} + \mathbf{q}_m|^2}$, projected along the xy plane and z axis, respectively.

Since we are mainly interested in fields that are scattered and which propagate away from the surface along the $\pm z$ directions, the z -projected wavenumber $\sqrt{k^2 - |\mathbf{k}_{\parallel} + \mathbf{q}_m|^2}$ has to be real (as opposed to the case of surface modes which are evanescent along z). This leads to the same conditions on the diffraction orders m as analyzed in the analytical calculation of $\bar{\Gamma}$, so that for the single diffraction order case, e.g. $a < \lambda/2$ in the square lattice case, we obtain

$$\lambda g_{sc,ij}(\mathbf{k}_{\parallel}, \mathbf{r}) = \frac{i}{4\pi} \left(\frac{\lambda}{a} \right)^2 \frac{k}{k_z} \left(\delta_{ij} - \xi_{ij} \frac{k_i k_j}{k^2} \right) e^{i\mathbf{k}_{\parallel} \cdot \mathbf{r}_{\parallel}} e^{ik_z|z|}. \quad (\text{S26})$$

The total field at $\mathbf{r} = (\mathbf{r}_{\parallel}, z)$ with $|z| \gtrsim a$ sufficiently far from the atomic array where the evanescent waves do not contribute, is then found by inserting the above $\bar{g}_{sc}(\mathbf{k}_{\parallel}, \mathbf{r})$ into Eq. (S23), yielding

$$\mathbf{E}(\mathbf{r}) = \left[e^{ik_z z} + \bar{S}_{\pm}(\mathbf{k}_{\parallel}) e^{-ik_z|z|} \right] e^{i\mathbf{k}_{\parallel} \cdot \mathbf{r}_{\parallel}} \mathbf{E}_{0,\mathbf{k}_{\parallel}}, \quad (\text{S27})$$

with the scattering matrix

$$\bar{S}_{\pm}(\mathbf{k}_{\parallel}) = \frac{4\pi^2}{\epsilon_0 \lambda^2} e^{-i\mathbf{k}_{\parallel} \cdot \mathbf{r}_{\parallel}} e^{-ik_z|z|} \bar{g}_{sc}(\mathbf{k}_{\parallel}, \mathbf{r}) \bar{\alpha}_e(\mathbf{k}_{\parallel}). \quad (\text{S28})$$

The subscript \pm in \bar{S}_{\pm} distinguishes between forward (+ sign for $z > 0$) and backward (- sign for $z < 0$) scattering. The fact that \bar{S}_{\pm} depends on the sign of z , without z explicitly appearing in it, is due to its dependence on ξ_{ij} which is sensitive to the sign of z (see explanations below Eq. S25).

It is constructive to analyze the scattering within the field polarization basis which is most natural for propagating plane waves, namely, that of the wavevector $\mathbf{k} = k \mathbf{e}_k$ and the transverse polarizations perpendicular to it. Eq. (S27) reveals that for an incoming plane wave with a wavevector $\mathbf{k} = (\mathbf{k}_{\parallel}, k_z)$, an additional wavevector $\mathbf{k}' = (\mathbf{k}_{\parallel}, -k_z)$ emerges for the backward scattered field (at $z < 0$) while the forward scattered field (at $z > 0$) possess the incident wavenumber \mathbf{k} . We can therefore define two relevant polarization basis, one for the incoming and transmitted fields and the other for reflected ones, $\{\mathbf{e}_k, \mathbf{e}_p^+, \mathbf{e}_s^+\}$ and $\{\mathbf{e}_{k'}, \mathbf{e}_p^-, \mathbf{e}_s^-\}$, respectively, with $\mathbf{e}_{p,s}^+ \perp \mathbf{e}_k$ and $\mathbf{e}_{p,s}^- \perp \mathbf{e}_{k'}$ (Fig. S1a). In spherical coordinates these basis vectors read

$$\begin{aligned} \mathbf{e}_k &= (\sin \theta \cos \phi, \sin \theta \sin \phi, \cos \theta), & \mathbf{e}_p^+ &= (\cos \theta \cos \phi, \cos \theta \sin \phi, -\sin \theta), & \mathbf{e}_s^+ &= (\sin \phi, -\cos \phi, 0); \\ \mathbf{e}_{k'} &= (\sin \theta \cos \phi, \sin \theta \sin \phi, -\cos \theta), & \mathbf{e}_p^- &= (-\cos \theta \cos \phi, -\cos \theta \sin \phi, -\sin \theta), & \mathbf{e}_s^- &= (\sin \phi, -\cos \phi, 0) \end{aligned} \quad (\text{S29})$$

where all column vectors here are written in cartesian basis, i.e. as (A_x, A_y, A_z) for a vector \mathbf{A} .

Writing $\bar{\bar{g}}_{sc}$ from Eq. (S26) as

$$\lambda \bar{\bar{g}}_{sc}(\mathbf{k}_{\parallel}, \mathbf{r}) = \frac{i}{4\pi} \left(\frac{\lambda}{a} \right)^2 \frac{k}{k_z} \bar{\bar{F}}_{\pm} e^{i\mathbf{k}_{\parallel} \cdot \mathbf{r}_{\parallel}} e^{ik_z|z|}, \quad (\text{S30})$$

with

$$F_{\pm,ij} = \delta_{ij} - \xi_{ij} k_i k_j / k^2 \quad (\text{S31})$$

being its tensor part (written in cartesian basis) and where the \pm subscript is due to the dependence of ξ_{ij} on the sign of z , we notice that the $\{\mathbf{e}_k, \mathbf{e}_p^+, \mathbf{e}_s^+\}$ and $\{\mathbf{e}_{k'}, \mathbf{e}_p^-, \mathbf{e}_s^-\}$ basis form the eigenvectors of $\bar{\bar{F}}_+$ and $\bar{\bar{F}}_-$, respectively, with eigenvalues $\{0, 1, 1\}$, respectively, for both \pm cases. Considering also that the incident field must posses one of two forward transverse polarizations $\mathbf{e}_{p,s}^+$, we can now describe the total field in Eq. (S27) via its components $E^\mu = \mathbf{e}_\mu \cdot \mathbf{E}$ projected onto the transverse polarization basis $\mu = \{p, s\}$,

$$E^\mu(\mathbf{r}) = \sum_{\nu=p,s} \left[\delta_{\mu\nu} e^{ik_z z} + S_{\mu\nu}^{\pm}(\mathbf{k}_{\parallel}) e^{ik_z|z|} \right] e^{i\mathbf{k}_{\parallel} \cdot \mathbf{r}_{\parallel}} E_{0,\mathbf{k}_{\parallel}}^\nu. \quad (\text{S32})$$

Here the scattering matrix is represented by its 2×2 matrix elements, $S_{\mu\nu}^{\pm} = \mathbf{e}_\mu^{\pm\dagger} \bar{\bar{S}} \mathbf{e}_\nu^{\pm}$, which are obtained from Eqs. (S28,S30) and the matrix elements $\mathbf{e}_\mu^{\pm\dagger} \bar{\bar{F}}_{\pm} \mathbf{e}_\nu^{\pm} = \delta_{\mu\nu}$ as

$$S_{\mu\nu}^{\pm}(\mathbf{k}_{\parallel}) = i\pi \left(\frac{\lambda}{a} \right)^2 \frac{k}{k_z} \frac{1}{\varepsilon_0 \lambda^3} \mathbf{e}_\mu^{\pm\dagger} \bar{\alpha}_e(\mathbf{k}_{\parallel}) \mathbf{e}_\nu^{\pm}. \quad (\text{S33})$$

The scattering properties of the array can then be further characterized by the intensity transmission and reflection matrices, $T_{\mu\nu} = |\delta_{\mu\nu} + S_{\mu\nu}^+|^2$ and $R_{\mu\nu} = |S_{\mu\nu}^-|^2$, where $\delta_{\mu\nu}$ is the Kronecker delta. Figure 3a of the main text shows that R_{ss} , for $a = 0.2\lambda$ and $\delta = 0$, exceeds 0.99 at all incident angles. In the case of p -polarization, reflection exceeds 0.95 for a wide range of angles, far beyond the paraxial approximation, as seen in Fig. S1b here. Furthermore, we find that mixing between polarizations is small $T_{sp}, T_{ps}, R_{sp}, R_{ps} \sim 10^{-3}$ (see Sec. 3.2 below), which demonstrates that the array operates as an excellent mirror for almost all incident angles and both incident polarizations.

At normal incidence we recall that $\bar{\alpha}_e$ is a scalar in the $\{x, y\}$ basis (which forms the $\{p, s\}$ -polarization basis). Then, $\bar{\bar{S}}$ is also a scalar $S_{\mu\nu} = S \delta_{\mu\nu}$ where S is given by Eq. (S33) with $k_z = k$ and with the scalar polarizability at normal incidence (see text below Eq. S14),

$$\alpha_e = -\frac{3}{4\pi^2} \varepsilon_0 \lambda_a^3 \frac{\gamma/2}{\delta - \Delta + i(\gamma + \gamma_{\text{nr}} + \Gamma)/2}, \quad (\text{S34})$$

yielding Eq. (3) in the main text.

2.4. Beyond single diffraction order

An additional diffraction order can appear when the lattice constant exceeds $\lambda/2$, since the addition of a reciprocal lattice vector, $\sim 2\pi/a$, to the incident wavevector due to Bragg scattering by the lattice, may now result in a propagating wave (Fig. S2a). This situation can be analyzed by a straightforward extension of the above formalism. Whereas for s -polarized light the resulting scattering is quite simple (Fig. 2Sb), new possibilities arise for p -polarization, where the propagation along certain directions is suppressed, such as the retro-reflection effect in Fig. 2Sc.

2.5. Quantum master equation formulation

We now extend our discussion to treat both the atoms and the electromagnetic field quantum mechanically. An isotropic atom must consist of at least four levels: a ground state $|g\rangle$ and three degenerate excited states $|i\rangle$, where $i = x, y, z$. The excited states are labeled by the direction of the dipole moment $\mathbf{d}_i = d\mathbf{e}_i$ associated with the transition $|g\rangle \rightarrow |i\rangle$, where \mathbf{e}_i is the unit vector along the i axis. We further define the atomic lowering operators $\hat{\sigma}_i = |g\rangle\langle i|$ and the corresponding raising operators $\hat{\sigma}_i^\dagger = |i\rangle\langle g|$. For an array of atoms, we require an additional index, $\hat{\sigma}_{mi}$, to label the site m of the atom. By tracing out over the photonic degrees of freedom and making the

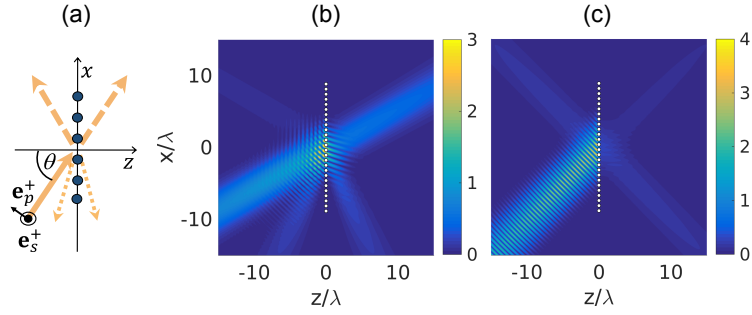


FIG. S2: (a) Scattering beyond a single diffraction order. Compared to Fig S1a, an additional diffraction order appears on both sides of the array. (b) Results of a numerical calculation (Sec. 6 below) for a \$s\$-polarized Gaussian beam of waist \$3\lambda\$ and \$\delta = \Delta\$, incident at a \$30^\circ\$ angle relative to the \$z\$ axis. The beam is scattered off an array of \$26 \times 26\$ atoms with \$a = 0.707\lambda\$. All field intensities are in units of \$|\mathbf{E}_0|^2\$. (c) Retro-reflector effect for the same array and incident Gaussian beam, this time \$p\$-polarized at an incident angle of \$45^\circ\$. Scattering is strongly suppressed into directions for which the \$p\$-polarization is orthogonal to the \$p\$-polarization of the incident beam. As a result, most of the light is back scattered into the first diffraction order, which is parallel to the incident beam.

Born–Markov approximation, one arrives at a quantum master equation describing the dynamics of the atoms [7, 8]. The master equation can be written in terms of the reduced density operator \$\rho(t)\$ as

$$\frac{d}{dt}\rho(t) = -i[H_S, \rho(t)] + \mathcal{D}[\rho(t)], \quad (\text{S35})$$

where

$$H_S = \sum_{m,i} \omega_a \sigma_{mi}^\dagger \sigma_{mi} + \sum_{m \neq n, i,j} \Delta_{ij}(\mathbf{r}_m, \mathbf{r}_n) \sigma_{mi}^\dagger \sigma_{nj} \quad (\text{S36})$$

captures the coherent dynamics, while

$$\mathcal{D}[\rho] = \sum_{m,n,i,j} \Gamma_{ij}(\mathbf{r}_m, \mathbf{r}_n) \left(\sigma_{mi}^\dagger \rho \sigma_{nj} - \frac{1}{2} \left\{ \sigma_{mi}^\dagger \sigma_{nj}, \rho \right\} \right) \quad (\text{S37})$$

corresponds to incoherent, dissipative evolution. The parameters \$\Delta_{ij}(\mathbf{r}_m, \mathbf{r}_n)\$ specify the coherent dipole–dipole interaction between two atoms, whereas \$\Gamma_{ij}(\mathbf{r}_m, \mathbf{r}_n)\$ denote the strength of their collective decay. These parameters can be expressed in terms of the dyadic Green’s function of free space as

$$\Delta_{ij}(\mathbf{r}_m, \mathbf{r}_n) = -\frac{3\pi\gamma c}{\omega_a} \text{Re}[G_{ij}(\omega_a, \mathbf{r}_m, \mathbf{r}_n)], \quad \Gamma_{ij}(\mathbf{r}_m, \mathbf{r}_n) = \frac{6\pi\gamma c}{\omega_a} \text{Im}[G_{ij}(\omega_a, \mathbf{r}_m, \mathbf{r}_n)]. \quad (\text{S38})$$

We note the sum involving \$\Delta_{ij}(\mathbf{r}_m, \mathbf{r}_n)\$ in Eq. (S36) excludes \$m = n\$ since this term merely corresponds to a renormalization of the transition frequency \$\omega_a\$ [9–11].

For an infinite atomic array with discrete translational symmetry, it is convenient to introduce the momentum space operators

$$\sigma_{\mathbf{k}i} = \sum_m \sigma_{mi} e^{i\mathbf{k} \cdot \mathbf{r}_m}, \quad \sigma_{mi} = A_0 \int_{\text{BZ}} \frac{d^2\mathbf{k}}{(2\pi)^2} \sigma_{\mathbf{k}i} e^{-i\mathbf{k} \cdot \mathbf{r}_m}. \quad (\text{S39})$$

where \$\mathbf{k}\$ is a 2D wavevector restricted to the first Brillouin zone of the reciprocal lattice and \$A_0\$ is the area of a unit cell. The Hamiltonian \$H_S\$ and the dissipator \$\mathcal{D}\$ may then be written as

$$H_S = A_0 \int_{\text{BZ}} \frac{d^2\mathbf{k}}{(2\pi)^2} \sum_{i,j} [\omega_a \delta_{ij} + \Delta_{ij}(\mathbf{k})] \sigma_{\mathbf{k}i}^\dagger \sigma_{\mathbf{k}j} \quad (\text{S40})$$

$$\mathcal{D}[\rho] = A_0 \int_{\text{BZ}} \frac{d^2\mathbf{k}}{(2\pi)^2} \sum_{i,j} [\gamma \delta_{ij} + \Gamma_{ij}(\mathbf{k})] \left(\sigma_{\mathbf{k}i}^\dagger \rho \sigma_{\mathbf{k}j} - \frac{1}{2} \left\{ \sigma_{\mathbf{k}i}^\dagger \sigma_{\mathbf{k}j}, \rho \right\} \right). \quad (\text{S41})$$

Here, we defined

$$\Delta_{ij}(\mathbf{k}) = \sum_{m \neq n} \Delta_{ij}(\mathbf{r}_m, \mathbf{r}_n) e^{i\mathbf{k} \cdot (\mathbf{r}_m - \mathbf{r}_n)}, \quad \Gamma_{ij}(\mathbf{k}) = \sum_{m \neq n} \Gamma_{ij}(\mathbf{r}_m, \mathbf{r}_n) e^{i\mathbf{k} \cdot (\mathbf{r}_m - \mathbf{r}_n)}, \quad (S42)$$

independent of n since $G(\omega_a, \mathbf{r}_m, \mathbf{r}_n)$ only depends on $\mathbf{r}_m - \mathbf{r}_n$. For a given momentum \mathbf{k} , the evolution of the atoms is thus specified by the two 3×3 matrices $\bar{\Delta}(\mathbf{k})$ and $\bar{\Gamma}(\mathbf{k})$. The former specifies the energies of the three Bloch modes with momentum \mathbf{k} , giving rise to a bandstructure, while the latter describes their decay.

The expressions for $\bar{\Delta}$ and $\bar{\Gamma}$ derived here are identical to those from the classical treatment. Of course, this is expected since the classical results should follow from the quantum treatment in the linear regime, where the atomic transitions are not saturated. Furthermore, the reflection and transmission coefficients computed from the linear response of the quantum system must agree with those obtained from the classical theory. One can show that this is indeed the case by introducing a driving term to the Hamiltonian, corresponding to an incident field, and computing the field radiated by the atoms.

3. PROPERTIES OF THE COOPERATIVE RESONANCE AND DECAY

3.1. Structure of the functions $\Delta(a)$ and $\Gamma(a)$ at normal incidence

Figure 2a of the main text presents Δ as a function of the lattice spacing a normalized to the incident wavelength λ . The general features of its dependence on a/λ can be elegantly explained by establishing its Kramers-Kronig relation with the function $\Gamma(a/\lambda)$. We recall the expressions for Δ and Γ at normal incidence (c.f. Eq. 4 in the main text or Eq. S15 here and text below it), which are in general functions of the incident frequency ω ($\lambda = 2\pi c/\omega$) and the lattice points

$$\Delta(\omega, a) = -\frac{3}{2}\gamma\lambda \sum_{n \neq 0} \text{Re}G_{xx}(\omega, 0, \mathbf{r}_n), \quad \Gamma(\omega, a) = 3\gamma\lambda \sum_{n \neq 0} \text{Im}G_{xx}(\omega, 0, \mathbf{r}_n). \quad (S43)$$

Since the dyadic Green's function is a linear response function (of the modes that form the electromagnetic field/vacuum), it satisfies the Kramers-Kronig relation,

$$\text{Re}G_{xx}(\omega, \mathbf{r}, \mathbf{r}') = \frac{1}{\pi} \int_{-\infty}^{\infty} d\omega' \frac{\text{Im}G_{xx}(\omega', \mathbf{r}, \mathbf{r}')}{\omega - \omega'}. \quad (S44)$$

Writing the position vector of an atom n as $\mathbf{r}_n = \mathbf{r}_{n_x, n_y} = a\mathbf{n}$ with $\mathbf{n} = (n_x \mathbf{e}_x + n_y \mathbf{e}_y)$ and considering the dyadic Green's function in free space, Eq. (S3), we note that ω and a always appear together as $2\pi\omega a/c = a/\lambda$ so that $\lambda G_{xx}(\omega, 0, \mathbf{r}_n)$ can be written as a function of only the dimensionless distance a/λ and the vector index \mathbf{n} (independent of a and ω). Therefore, the Kramers-Kronig relation, Eq. (S44), for $G_{xx}(\omega, 0, \mathbf{r}_n)$ can be written as

$$\text{Re}[\lambda G_{xx}(a/\lambda, \mathbf{n})] = \frac{1}{\pi} \int_{-\infty}^{\infty} du \frac{\text{Im}[\lambda G_{xx}(u, \mathbf{n})]}{a/\lambda - u}. \quad (S45)$$

Inserting this relation into the expression for Δ in Eq. (S43) and performing the sum over n , the dependence on \mathbf{n} disappears and we obtain a Kramers-Kronig relation between the real and imaginary part of the field response as a function of the scaled lattice spacing a/λ

$$\Delta(a/\lambda) = -\frac{1}{\pi} \int_{-\infty}^{\infty} du \frac{\Gamma(u)/2}{a/\lambda - u}, \quad (S46)$$

where both $\Delta(u)$ and $\Gamma(u)$ are now understood to be functions of a single variable $u = a/\lambda$.

Turning now to the structure of the function $\Delta(a/\lambda)$ we begin with the region $a/\lambda \ll 1$. In this limit the sum over n in Eq. (S43) can be converted into an integral and we analytically find $\Delta \propto 1/a^3$ which agrees with the divergence near $a/\lambda \rightarrow 0^+$ in Fig. 2a of the main text and Fig. S3 here (see also Ref. [12]). This $1/a^3$ scaling is easily understood by recalling that the real part of the Green's function Eq. (S3), amounting to dipole-dipole interaction, scales as $1/r^3$ at the quasistatic, short distance limit, and that Δ is a sum over such dipole-dipole interactions. In order to explain the behavior of $\Delta(a/\lambda)$ at all regions beyond the $a/\lambda \ll 1$ we resorted to the Kramers-Kronig relation Eq. (S46), for which we need to consider the function $\Gamma(a/\lambda)$. For $a/\lambda < 1$ we have obtained an analytical expression for Γ (Eq.

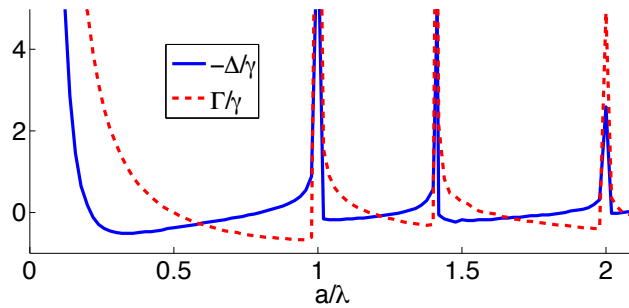


FIG. S3: Cooperative shift Δ and width Γ as a function of a/λ at normal incidence (extension of Fig. 2a in the main text; results obtained by a direct summation of Eq. (4) in the main text). The diffraction-orders-associated peaks and the Kramers-Kronig structure of the relation between the Δ and Γ as a function of the scaled lattice constant a/λ are clearly seen (see text, Sec. 3.3.1).

4 in main text) by using the fact that there exists only one diffraction order in the scattered light. In other words, the reservoir established by the free-space vacuum, forms only a single radiative *dissipation channel* for the atomic array at $a/\lambda < 1$, imposing a decay rate Γ which results only from the term $m_x, m_y = 0$ in Eq. (S21). For $a/\lambda = 1$, additional dissipation channels arise in the form of emission to the directions (diffraction orders) $|m_x| = 1, m_y = 0$ and $|m_y| = 1, m_x = 0$. This physically explains the peak observed in $\Gamma(a/\lambda)$ for $a/\lambda = 1$ in Fig. S3 (mathematically, additional poles contribute to the imaginary part of the sum in Eq. S21). The meaning is that whenever a new dissipation channel appears, in the form of a new diffraction order in the far field, we expect a peak in $\Gamma(a/\lambda)$. Indeed, this can be seen in Fig. S3 by the additional peaks at $a/\lambda = \sqrt{2}$ (diffraction orders $|m_x| = |m_y| = 1$) and $a/\lambda = 2$ (diffraction orders $|m_x| = 2, m_y = 0$ and $|m_y| = 2, m_x = 0$). In turn, these peaks in $\Gamma(a/\lambda)$ physically explain the corresponding dispersive-like peaks in $\Delta(a/\lambda)$ following the Kramers-Kronig relation Eq. (S46), nicely seen in Fig. S3 (whereas Fig. 2a in the main text captures only the $a/\lambda = 1$ dispersive peak).

3.2. Polarization eigenbasis of $\bar{\bar{\Delta}}$ and $\bar{\bar{\Gamma}}$

For $a < \lambda/2$, we derived an explicit expression for $\bar{\bar{\Gamma}}(\mathbf{k}_{\parallel})$ in Eq. (S22). Written in terms of spherical coordinates θ and ϕ , the expression becomes

$$\bar{\bar{\Gamma}}(\mathbf{k}_{\parallel}) = \frac{3\gamma}{4\pi \cos \theta} \left(\frac{\lambda}{a} \right)^2 \begin{pmatrix} 1 - \sin^2 \theta \cos^2 \phi & -\sin^2 \theta \cos \phi \sin \phi & 0 \\ -\sin^2 \theta \cos \phi \sin \phi & 1 - \sin^2 \theta \sin^2 \phi & 0 \\ 0 & 0 & \sin^2 \theta \end{pmatrix} - \gamma \begin{pmatrix} 1 & 0 & 0 \\ 0 & 1 & 0 \\ 0 & 0 & 1 \end{pmatrix}. \quad (\text{S47})$$

The matrix can be straightforwardly diagonalized. One obtains the three eigenvalues

$$\Gamma_1 = \frac{3\gamma \cos \theta}{4\pi} \left(\frac{\lambda}{a} \right)^2 - \gamma, \quad \Gamma_2 = \frac{3\gamma}{4\pi \cos \theta} \left(\frac{\lambda}{a} \right)^2 - \gamma, \quad \Gamma_3 = \frac{3\gamma \sin^2 \theta}{4\pi \cos \theta} \left(\frac{\lambda}{a} \right)^2 - \gamma, \quad (\text{S48})$$

with the respective eigenvectors

$$\mathbf{v}_1 = (\cos \phi, \sin \phi, 0) = \mathbf{k}_{\parallel}/|\mathbf{k}_{\parallel}|, \quad \mathbf{v}_2 = (-\sin \phi, \cos \phi, 0) = \mathbf{e}_s, \quad \mathbf{v}_3 = (0, 0, 1) = \mathbf{e}_z. \quad (\text{S49})$$

We observe that \mathbf{v}_2 points along the direction of *s*-polarized incident light, while \mathbf{v}_1 and \mathbf{v}_3 are superpositions of the *p*-polarization and a longitudinal component.

The cooperative shift $\bar{\bar{\Delta}}(\mathbf{k}_{\parallel})$ has the same block-diagonal structure as $\bar{\bar{\Gamma}}(\mathbf{k}_{\parallel})$, such that $\mathbf{v}_3 = (0, 0, 1)$ is also an eigenvector of $\bar{\bar{\Delta}}(\mathbf{k}_{\parallel})$. The other two eigenvectors, which we denote by $\mathbf{w}_{1,2}$, are in general different. However, it turns out that they are approximately equal to $\mathbf{v}_{1,2}$ as demonstrated in Fig. S4. As a result, the *s*-polarization is an approximate eigenvector of both $\bar{\bar{\Gamma}}$ and $\bar{\bar{\Delta}}$ and hence of the scattering matrix. This further implies that the surface only weakly mixes the *s*- and *p*-polarizations. Indeed, for $a/\lambda = 0.2$, the reflection coefficient R_{sp} never exceeds 4×10^{-3} as shown in Fig. S4c ($R_{sp} = R_{ps}$ by symmetry).

The above discussion of the eigenvectors of $\bar{\bar{\Delta}}$ and $\bar{\bar{\Gamma}}$ also explains why the matrix element Δ_{ss} alone is sufficient to predict the reflection coefficient R_{ss} to a good approximation (see main text). By contrast, no such simple

explanation is available for the p -polarization since it forms a superposition of \mathbf{w}_1 and \mathbf{e}_z . Nevertheless, for small enough incident angles within the paraxial regime where $\mathbf{e}_p^\pm \approx \pm \mathbf{k}_{\parallel}/|\mathbf{k}_{\parallel}| \approx \pm \mathbf{w}_1$, the p -polarization becomes an approximate eigenvector of $\bar{\Gamma}$ and $\bar{\Delta}$. The plot of $\Delta_{pp} = \mathbf{e}_p^{-\dagger} \bar{\Delta} \mathbf{e}_p^+$ in Fig. 1Sc then exhibits a resonance ($\Delta_{pp} \approx 0 = \delta$) matching that of R_{pp} within the paraxial regime, but fails to reproduce many qualitative features of R_{pp} .

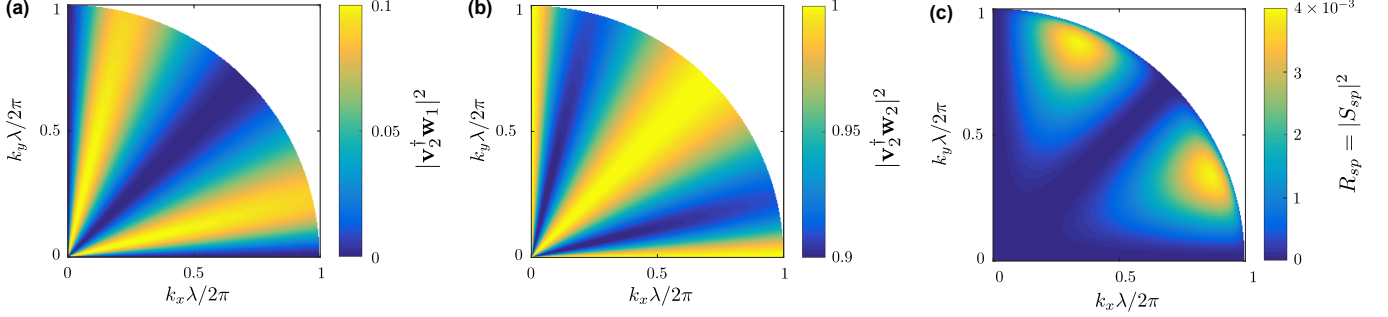


FIG. S4: Overlap between the two in-plane eigenvectors \mathbf{w}_1 and \mathbf{w}_2 of $\bar{\Delta}$ and one of the in-plane eigenvectors \mathbf{v}_2 of $\bar{\Gamma}$. (a) indicates that \mathbf{w}_1 is approximately orthogonal to \mathbf{v}_2 for all \mathbf{k}_{\parallel} inside the light cone. Similarly, it is evident from (b) that \mathbf{w}_2 is approximately parallel to \mathbf{v}_2 . (c) Off-diagonal reflection coefficient R_{sp} (due to symmetry, $R_{sp} = R_{ps}$). All plots were computed for lattice constant $a/\lambda = 0.2$.

4. DISORDERED ARRAYS

Disorder in atomic positions can be described by writing $\mathbf{r} = \mathbf{r}_n^0 + \delta\mathbf{r}_n$ for the position of an atom n , where \mathbf{r}_n^0 are the ordered lattice positions and $\delta\mathbf{r}_n$ are a small random fluctuations. The effect on the self-consistent scattering equation, Eq. (S6), is a perturbation of the Green's function,

$$\bar{\bar{G}}_{nm} = \bar{\bar{G}}(\mathbf{r}_n - \mathbf{r}_m) = \bar{\bar{G}}_{nm}^{(0)} + \bar{\bar{\delta G}}_{nm}, \quad (\text{S50})$$

with $\bar{\bar{G}}_{nm}^{(0)} = \bar{\bar{G}}(\mathbf{r}_n^0 - \mathbf{r}_m^0)$ the disorder-free component. The perturbation $\bar{\bar{\delta G}}_{nm}$ is expanded in orders $\delta r/a$, where δr is the typical scale for the fluctuations $\delta\mathbf{r}_n$ and a is the lattice spacing,

$$\begin{aligned} \bar{\bar{\delta G}}_{nm} &= \bar{\bar{\delta G}}_{nm}^{(1)} + \bar{\bar{\delta G}}_{nm}^{(2)} + \dots \\ &= \sum_{i=x,y,z} \frac{\partial}{\partial r^i} \bar{\bar{G}}(\mathbf{r}) \Big|_{\mathbf{r}_n^0 - \mathbf{r}_m^0} \delta r_{nm}^i + \frac{1}{2} \sum_i \sum_j \frac{\partial}{\partial r^i} \frac{\partial}{\partial r^j} \bar{\bar{G}}(\mathbf{r}) \Big|_{\mathbf{r}_n^0 - \mathbf{r}_m^0} \delta r_{nm}^i \delta r_{nm}^j + \dots, \end{aligned} \quad (\text{S51})$$

with $\delta r_{nm}^i = \mathbf{e}_i \cdot (\delta\mathbf{r}_n - \delta\mathbf{r}_m)$. Similarly, we can write for the polarization, $\mathbf{p}_n = \mathbf{p}_n^{(0)} + \delta\mathbf{p}_n$, where $\mathbf{p}_n^{(0)}$ is the self-consistent solution in the ordered case, and insert it into Eq. (S6), yielding

$$\delta\mathbf{p}(\mathbf{k}_{\parallel}) = \frac{4\pi^2\alpha}{\varepsilon_0\lambda^2} \sum_{\mathbf{k}'_{\parallel}} \left\{ \bar{\bar{\delta g}}(\mathbf{k}_{\parallel}, \mathbf{k}'_{\parallel}) \mathbf{p}^{(0)}(\mathbf{k}'_{\parallel}) + \left[\bar{\bar{g}}^{(0)}(\mathbf{k}_{\parallel}) \delta_{\mathbf{k}_{\parallel}, \mathbf{k}'_{\parallel}} + \bar{\bar{\delta g}}(\mathbf{k}_{\parallel}, \mathbf{k}'_{\parallel}) \right] \delta\mathbf{p}(\mathbf{k}'_{\parallel}) \right\}, \quad (\text{S52})$$

with $\mathbf{p}(\mathbf{k}_{\parallel}) = (1/N) \sum_n e^{-i\mathbf{k}_{\parallel} \cdot \mathbf{r}_n^0} \mathbf{p}_n$ and $\bar{\bar{\delta g}}(\mathbf{k}_{\parallel}, \mathbf{k}'_{\parallel}) = (1/N) \sum_n \sum_{m \neq n} e^{-i\mathbf{k}_{\parallel} \cdot \mathbf{r}_n^0} \bar{\bar{G}}_{nm} e^{i\mathbf{k}'_{\parallel} \cdot \mathbf{r}_m^0}$, and where $\bar{\bar{g}}^{(0)}(\mathbf{k}_{\parallel})$ is the disorder-free tensor from Eq. (S12). The above self-consistent equation for the perturbation $\delta\mathbf{p}(\mathbf{k}_{\parallel})$ serves as the starting point for a perturbation theory with the small parameter $\delta r/a$, upon considering the formal expansion $\delta\mathbf{p}(\mathbf{k}_{\parallel}) = \delta\mathbf{p}^{(1)}(\mathbf{k}_{\parallel}) + \delta\mathbf{p}^{(2)}(\mathbf{k}_{\parallel}) + \dots$ together with the expansion of Eq. (S51).

For a simple estimation of the effect of disorder, we take statistically independent and identically-distributed fluctuations δr_n^i with zero mean and variance δr^2 ,

$$\langle \delta r_n^i \rangle = 0, \quad \langle \delta r_n^i \delta r_m^j \rangle = \delta r^2 \delta_{nm} \delta_{ij}. \quad (\text{S53})$$

Using the above statistics in Eq. (S52), we can find disorder-induced corrections to the effective polarizability. For the cooperative resonance tensor Δ , we find to lowest order in $\delta r/a$ that the average of its disorder-induced correction vanishes, whereas its standard deviation scales as $(\delta r/\lambda)\Delta$.

By applying a similar perturbative treatment to Eq. (S5), we can also find the disorder-induced corrections to the scattered field. We find that to lowest order, the correction to the intensity reflection coefficient scales as $(\delta r/a)^2$.

For disorder due to impurities, we consider the case of an absence or addition of an atom in the array. We find numerically (see Sec. 5 below) that for small values of a/λ (e.g. 0.2) the results are almost unchanged compared with those of a perfect lattice, whereas for a/λ larger than 1/2 (e.g. 0.8) they may change considerably.

5. DIRECT NUMERICAL APPROACH TO THE SCATTERING PROBLEM

The problem of scattering of an electromagnetic field by a finite collection of point dipoles, generally formulated by Eqs. (S5) and (S6) can be solved numerically by a simple matrix inversion. Introducing the vector notation \bar{E} for the $3N$ -dimensional vector $E_i^n = p_i^n/\alpha$ (3 first entries are the 3 vector components of the E -field at the position of atom 1, next 3 are the field components at atom 2, etc.) and the notation $\bar{\mathbb{G}}$ for the $3N \times 3N$ matrix G_{ij}^{nm} , the solution of Eq. (S6) for the local fields on the atoms, $\bar{E} = E_i(\mathbf{r}_n)$, is

$$\bar{E} = \left[1 - 4\pi^2 \frac{\alpha}{\epsilon_0 \lambda^3} \lambda \bar{\mathbb{G}} \right]^{-1} \bar{E}_0. \quad (\text{S54})$$

Given the collection of atomic positions that form the array \mathbf{r}_n (e.g. square lattice), the incident field $\mathbf{E}_0(\mathbf{r})$ (see below) and the polarizability $\alpha(\omega)$ [Eq. S8], we can numerically invert the matrix in Eq. (S54). Then, we insert the solutions $\bar{E} = E_i^n = E_i(\mathbf{r}_n)$ into the right-hand side of Eq. (S5) and obtain the solution for the field at any given point \mathbf{r} , $E_i(\mathbf{r})$.

In order to compare the results of our analytical theory to those obtained numerically in a more realistic scenario, the infinite array is replaced by a finite square lattice of N atoms whereas all incident plane waves are replaced by Gaussian beams,

$$\mathbf{E}_0(x', y', z') = E_0 \mathbf{e}_L \frac{w_0}{w(z')} e^{ikz'} e^{-i\varphi(z')} e^{-\frac{x'^2+y'^2}{w^2(z')}} e^{ik\frac{x'^2+y'^2}{2R(z')}}, \quad (\text{S55})$$

with the usual beam parameters,

$$w(z) = w_0 \sqrt{1 + \left(\frac{z}{z_R} \right)^2}, \quad z_R = \frac{\pi w_0^2}{\lambda}, \quad R(z) = z \left[1 + \left(\frac{z_R}{z} \right)^2 \right], \quad \varphi(z) = \arctan \left(\frac{z'}{z_R} \right). \quad (\text{S56})$$

and where w_0 is the beam waist at its focal point and \mathbf{e}_L its polarization. Here the coordinates (x', y', z') are written in the reference frame of the beam, namely, where the beam propagates along the z' direction, $\mathbf{e}_k = \mathbf{e}_{z'}$. For normal incident Gaussian beam we have $x = x', y = y', z = z'$ and a polarization $\mathbf{e}_L \in \{\mathbf{e}_x, \mathbf{e}_y\}$, whereas for a beam propagating along the xz -plane at an angle θ from the z axis, we find

$$x' = x \cos \theta - z \sin \theta, \quad y' = y, \quad z' = z \cos \theta + z \sin \theta, \quad (\text{S57})$$

and

$$\mathbf{e}_L \in \{\mathbf{e}_p, \mathbf{e}_s\}, \quad \text{with} \quad \mathbf{e}_p = \cos \theta \mathbf{e}_x - \sin \theta \mathbf{e}_z, \quad \mathbf{e}_s = -\mathbf{e}_y. \quad (\text{S58})$$

For a faithful comparison with the infinite array case assumed in the theory, the cross section of the Gaussian beam at the position of the array, $z = 0$, has to be sufficiently smaller than the area of the array, Na^2 . At normal incidence ($\theta = 0$) we then always take $w_0 \leq 0.3a\sqrt{N}$, whereas for a general angle θ the waist w_0 has to be smaller by roughly $\cos \theta$.

Figs. S5 and S6 illustrate the excellent qualitative and quantitative agreement between this numerical solution and the theoretical results presented in the main text, both for the normal incident and oblique incident cases, respectively.

- [1] F. J. García de Abajo, Rev. Mod. Phys. **79**, 1267 (2007).
- [2] L. Novotny and B. Hecht, *Principles of Nano-Optics* (Cambridge University Press, 2006).
- [3] D. P. Craig and T. Thirunamachandran, *Molecular Quantum Electrodynamics* (Academic, London, 1984).
- [4] P. Lambropoulos and D. Petrosyan, *Fundamentals of Quantum Optics and Quantum Information* (Springer, 2007).

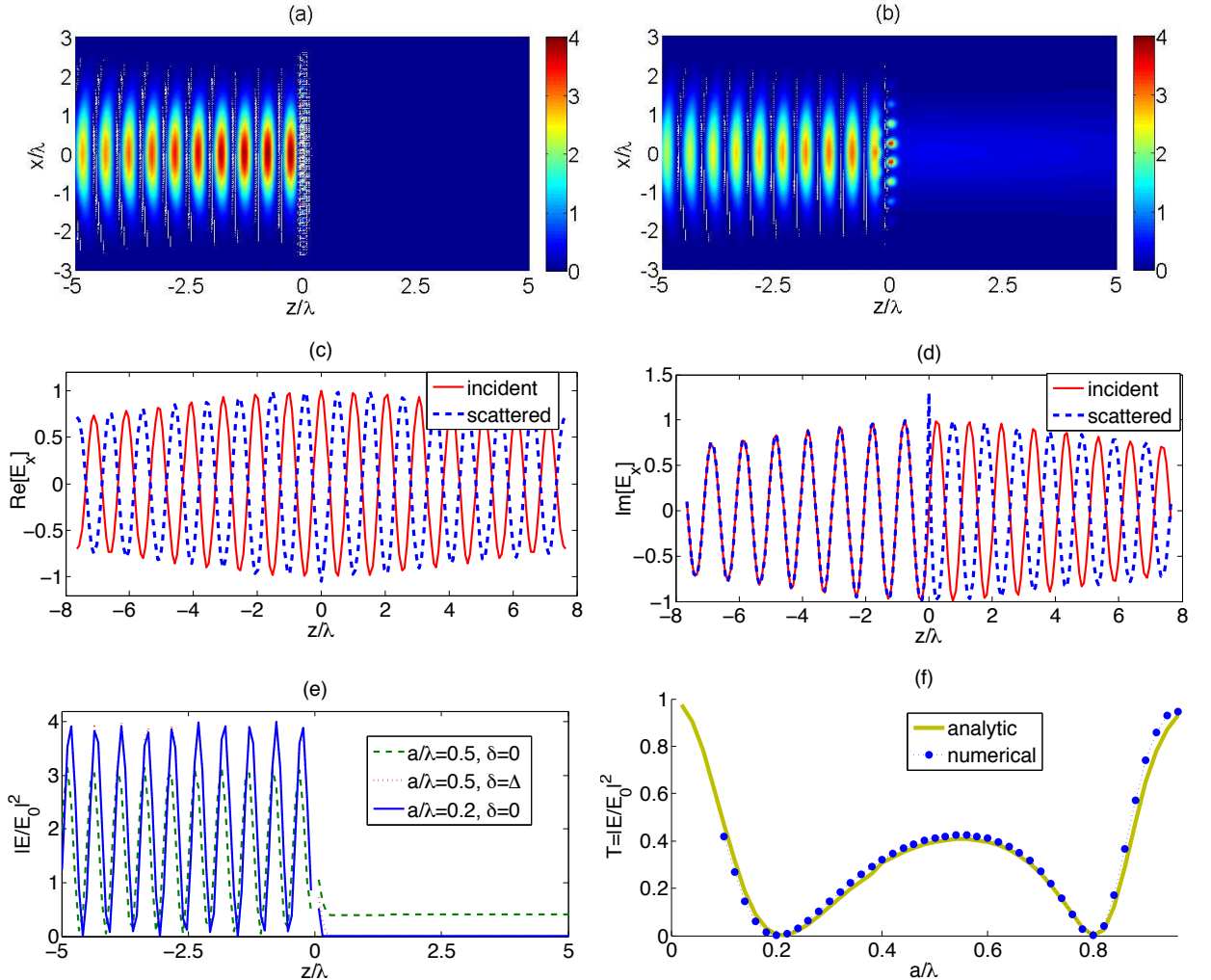


FIG. S5: Numerical approach, normal incidence. (a) x -polarized incident Gaussian beam at normal incidence to an array of $N = 26 \times 26$ atoms with a lattice constant $a = 0.2\lambda$ at $z = 0$. The incident beam is resonant with the bare atom, $\delta = 0$, and its waist is $w_0 = 0.3\sqrt{N}a = 1.56\lambda$. In agreement with Fig. 1c of the main text, no transmission is observed, and the reflected wave forms a standing wave with the incident field. All fields intensities are in units of $|E_0|^2$, the peak intensity of the incident Gaussian beam, Eq. (S55). (b) Same as (a) for $a = 0.5\lambda$ and $w_0 = 0.3\sqrt{N} \times 0.2 = 1.56\lambda$. Here, some of the field is transmitted as in Fig. 1c (main text). (c) A closer look at the scattering and interference processes for the case plotted in (a). Here we plot the incident and scattered field along z for a constant arbitrary value of x and y ($x = y = 0.2a$). The real part of the scattered field is exactly opposite in sign with respect to the real part of the incident field thus exactly cancelling it (all fields in units of E_0). (d) Same as (c) for the imaginary part of the field. For $z > 0$, beginning at a short distance after evanescent fields have decayed, there exists again exact cancellation, so that no transmitted (real and imaginary) field exists. For $z < 0$ the scattered field is equal and in phase with the incident field, amounting for perfect reflection and a standing wave. (e) Same as (c), this time the blue solid curve presents the total field intensity, showing the standing wave due to perfect reflection and zero transmission. The dashed green curve presents the same calculation for $a = 0.5\lambda$ where at $\delta = 0$ a transmission of about ~ 0.4 is observed in agreement with Fig. 1c of the main text. However, vanishing transmission (perfect reflection) can be achieved also at $a = 0.5\lambda$ by choosing the frequency of the incident field to match the cooperative resonance $\delta = \Delta$, which is found for $a = 0.5\lambda$ using Fig. 2a in the main text. The result is presented by the red dotted line which almost exactly coincides with the blue curve apart from the somewhat longer evanescent tail at $z > 0$ (which grows with a). (f) Transmitted field as a function of lattice spacing a/λ . Repeating the calculation from (d) for different a values at the individual-atomic resonance, $\delta = 0$, the transmission coefficient is extracted. For each a value the Gaussian beam waist is taken to be $w_0 = 0.3\sqrt{N}a$, i.e. smaller than the size of the array (blue dots). This nevertheless limits a/λ to be above 0.1 in order to keep $w_0 > \lambda/2$ (for the paraxial approximation to be valid). Excellent agreement with the analytical calculations for an infinite array and a plane wave, Fig. 1c in the main text which is reproduced here (green solid curve), is observed.

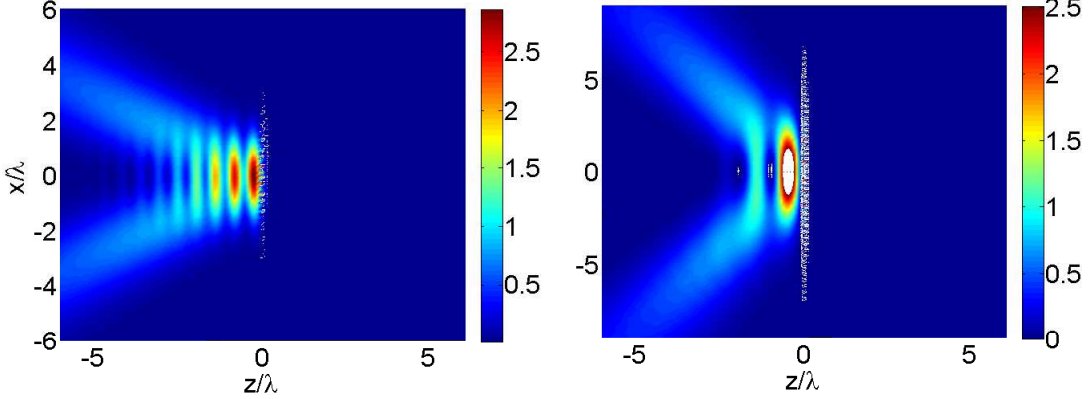


FIG. S6: Numerical approach, oblique incidence. (a) Reflection of a p -polarized Gaussian beam at an incident angle of $\theta = 30^\circ$. The beam waist is $w_0 = 1.56\lambda$ and the array contains 40×40 atoms with separation $a = 0.2$. In accordance with the theoretical predictions (Fig. S1 here), almost perfect reflection is observed. Quantitative agreement to the theory is found by examining the amplitude of the numerically calculated field along the x -axis at the far field, e.g. at $z = -6\lambda$ (noting the interference between the incident and reflected fields closer to the surface). (b) Same as (a) for s -polarized beam at an incident angle $\theta = 60^\circ$. Due to the larger angle of incidence, a larger array of 70×70 is taken, so that diffraction from the edges becomes very small and agreement to the theory (Fig. 3 in the main text) is observed.

- [5] The sum diverges due to the contribution of the Lamb shift whose counter term, the real part of $G_{ij}(0,0)$, was neglected here. In order to use these sums to obtain the real part of g_{ij} , we restore the real part of $G_{ij}(0,0)$, and represent it by an integral in momentum space which has a similar divergence as the sum on m . Then, by regularizing both the sum and the integral with the same, e.g. exponential/Gaussian cutoff function, the difference of the two converges numerically and yields the same results obtained by the direct summation in real space, Eq. (S12).
- [6] M. O. Scully and M. S. Zubairy, *Quantum Optics* (Cambridge University Press, 1997).
- [7] R. H. Lehmberg, Phys. Rev. A 2, 883 (1970).
- [8] M. Kiffner, M. Macovei, J. Eversb and C. H. Keitel, Progress in Optics **55**, pages 85-197 (2010).
- [9] P. de Vries, D. V. van Coevorden, and A. Lagendijk, Rev. Mod. Phys. **70**, 447 (1998).
- [10] J. A. Klugkist, M. Mostovoy, and J. Knoester, Phys. Rev. Lett. **96**, 1 (2006).
- [11] M. Antezza and Y. Castin, Phys. Rev. A **80**, 13816 (2009).
- [12] S. Thongrattanasiri, F. H. L. Koppens and F. J. García de Abajo, Phys. Rev. Lett. **108**, 047401 (2012).
- [13] R. J. Bettles, S. A. Gardiner and C. S. Adams, Phys. Rev. Lett. **116**, 103602 (2016).